

Ca²⁺-activated K⁺ channels reduce network excitability, improving adaptability and energetics for transmitting and perceiving sensory information

Xiaofeng Li,^{1,2,5} Ahmad Abou Tayoun^{3,5}, Zhuoyi Song^{2,5}, An Dau^{2,5}, Diana Rien^{1,5}, David Jaciuch², Sidhartha Dongre², Florence Blanchard², Anton Nikolaev², Lei Zheng², Murali K. Bollepalli⁴, Brian Chu⁴, Roger C. Hardie⁴, Patrick J. Dolph^{3*} and Mikko Juusola^{1,2*}

¹State Key Laboratory of Cognitive Neuroscience and Learning, Beijing Normal University, Beijing 100875, China

²Department of Biomedical Science, University of Sheffield, Sheffield S10 2TN, UK

³Department of Biology, Dartmouth College, Hanover, New Hampshire, USA

⁴Department of Physiology, Development, and Neuroscience, University of Cambridge, Cambridge CB2 3DY, UK

⁵These authors contributed equally to this work

*Correspondence: M.Juusola@Sheffield.ac.uk or Patrick.Dolph@dartmouth.edu

Highlights

- Homeostatic plasticity in *Drosophila* *dSlo*⁻, *dSK*⁻ and *dSK*⁻;*dSlo*⁻ null-mutants retains R1-R6 photoreceptors' light information sampling while reducing other K⁺-conductances
- As mutant R-LMC-R circuits rebalance synaptic loads homeostatically, R1-R6s become more depolarized, with *dSK*⁻ and *dSK*⁻;*dSlo*⁻ responding faster and *dSlo*⁻ slower, whilst LMC outputs oscillate, with *dSK*⁻ responding faster and *dSK*⁻;*dSlo*⁻ and *dSlo*⁻ slower than wild-type
- Homeostatic compensation in the mutant circuits impedes adaptation, increases the energy cost of visual information and distorts optomotor behavior
- Hence, Ca²⁺-activated K⁺ channels improve adaptability and energetics for transmitting and perceiving sensory information

SUMMARY

Ca²⁺-activated K⁺ channels (BK and SK) are ubiquitous in synaptic circuits, but their role in network adaptation and sensory perception remains largely unknown. Using electrophysiological and behavioral assays and biophysical modelling, we discover how visual information transfer in mutants lacking the BK channel (*dSlo*⁻), SK channel (*dSK*⁻) or both (*dSK*⁻;*dSlo*⁻) is shaped in the *Drosophila* R1-R6 photoreceptor-LMC circuits (R-LMC-R system) through synaptic feedforward-feedback interactions and reduced R1-R6 Shaker and Shab K⁺ conductances. This homeostatic compensation is specific for each mutant, leading to distinctive adaptive dynamics. We show how these dynamics inescapably increase the energy cost of information and distort the mutants' motion perception, determining the true price and limits of homeostatic compensation in an *in vivo* genetic animal model. These results reveal why Ca²⁺-activated K⁺ channels reduce network excitability (energetics), improving neural adaptability for transmitting and perceiving sensory information.

INTRODUCTION

Ca²⁺-activated K⁺ channels are widely expressed in both the visual system and CNS and play important roles in cell physiology, such as modulating neuronal excitability and neurotransmitter release. Based upon their kinetics, pharmacological and biophysical properties, these channels can be divided into two main types: the "small"- (SK; 2-20 pS) and "big"-conductance (BK; 200-400 pS)

channels. The SK channels are solely Ca^{2+} -activated (Faber and Sah, 2003; Sah, 1996; Salkoff, 2006; Stocker, 2004), while BK channels are both Ca^{2+} - and voltage-dependent. At synapses, SK channels form negative feedback loops with Ca^{2+} sources and are therefore essential regulators of synaptic transmission (Faber et al., 2005; Ngo-Anh et al., 2005). The functional role of BK channels in synaptic activities is less well understood, with various effects of blocking BK channels on neurotransmitter release having been reported (Fettiplace and Fuchs, 1999; Ramanathan et al., 1999; Xu and Slaughter, 2005).

Although Ca^{2+} -activated K^+ channels – through regulation of synaptic transmission between retinal neurons – seem to have conserved roles in early vertebrate (Clark et al., 2009; Grimes et al., 2009; Klocker et al., 2001; Pelucchi et al., 2008; Shatz, 1990; Wang et al., 1999) and invertebrate vision (Abou Tayoun et al., 2011), it has been difficult to work out how these channels advance *in vivo* circuit functions and what are their evolutionary benefits. This is because homeostatic processes that regulate electrical activity in neurons, in part, make communication in circuits surprisingly fault-tolerant against perturbations (Lemasson et al., 1993; Marder and Goaillard, 2006). Thus, the physical consequences of altering K^+ channel densities and those of homeostatic compensation are interconnected. Because *Drosophila* has single SK (*dSK*) and BK (*dSlo*) genes, electrophysiologically accessible photoreceptors and interneurons (Juusola and Hardie, 2001b; Zheng et al., 2006) with stereotypical connectivity (Meinertzhagen and O'Neil, 1991; Rivera-Alba et al., 2011), and readily quantifiable optomotor behavior (Blondeau and Heisenberg, 1982; Juusola et al., 2017), it provides an excellent model system to characterize how Ca^{2+} -activated K^+ channels affect circuit functions and the capacity to see. Here, we study to what extent intrinsic perturbations of missing one or both of these K^+ channels, through gene-deletion, can be neutralized by homeostatic processes trying to sustain normal network functions, and what is the price of this compensation.

By using electrophysiological and behavioral assays and biophysical modelling, we uncover why Ca^{2+} -activated K^+ channels improve communication between photoreceptors and Large Monopolar Cells (LMCs), which in the fly eye lamina network form stereotypical columns of feedforward and feedback synapses (R-LMC-R system) that process and route visual information to the fly brain. We show that although the loss of SK and BK channels does not diminish *Drosophila* photoreceptors' information sampling capacity *in vivo*, it homeostatically reduces other K^+ currents and overloads synaptic-feedback from the lamina network. This makes communication between the mutant photoreceptors and LMCs inefficient, consuming more energy and distorting visual information flow to the brain. Thus, homeostatic compensation of missing SK and BK channels within the lamina network is suboptimal and comes with an unavoidable cost of reduced adaptability and altered (accelerated or decelerated) vision, which is reflected by the mutant flies' uniquely tuned optomotor behaviors.

These results quantify the benefits of Ca^{2+} -activated K^+ channels in improving robustness, economics and adaptability of neural communication and perception.

RESULTS

Absence of *dSK* and *dSlo* Shapes Photoreceptor Responses

To examine how Ca^{2+} -activated K^+ channels shape *Drosophila* photoreceptor voltage output, we performed *in vivo* intracellular recordings (Figure 1A) from R1-R6 somata (Figure 1B) in the retinae

of $dSlo^-$, dSK^- and $dSK^-;dSlo^-$ null mutants and wild-type flies, using conventional sharp microelectrodes. Briefly dark-adapted (~20 s) mutant R1-R6s responded to logarithmically brightening light flashes with increasing graded depolarizations (Figure 1C), having wild-type-like or slightly smaller amplitudes (Figure 1D). However, both dSK^- and $dSK^-;dSlo^-$ R1-R6 outputs peaked faster (Figure 1E; mean time-to-peak) and decayed earlier (Figure 1F; mean half-width) to their respective resting potentials than the wild-type. While those of $dSlo^-$ R1-R6s, in contrast, showed decelerated dynamics, lasting longer than the wild-type except at the highest intensities (Figures 1C and 1F).

Notably, however, in all the corresponding recordings, the early light-induced depolarizations (Figure 1C; light grey area) were similar, implying that the mutant R1-R6s sampled light information normally. Thus, phototransduction reactions inside a R1-R6's ~30,000 microvilli (photon sampling units; Figure 1B), which form its light-sensor, the rhabdomere (Hardie and Juusola, 2015), seemed unaffected by the absence of Ca^{2+} -activated K^+ channels. But, instead, these mutant genotypes influenced more the subsequent neural information modulation phase (Figure 1C; light brown area).

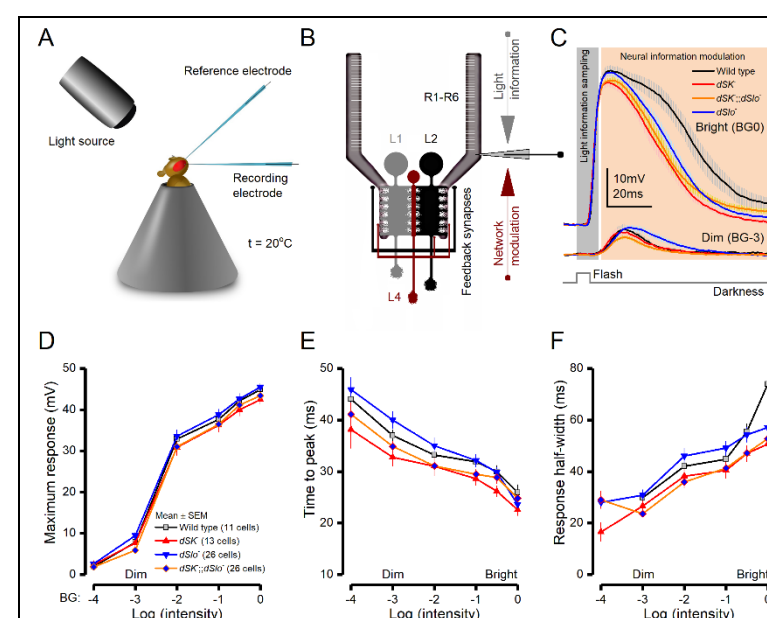


Figure 1. R1-R6 Photoreceptors of Different Ca^{2+} -Activated K^+ Channel Null-Mutants Show Distinctive Response Dynamics to Light Flashes

(A) Recordings were performed *in vivo* from R1-R6 somata using conventional sharp microelectrodes.

(B) 30,000 microvilli, which form a R1-R6's light-sensor, the rhabdomere (comb-like structure), sample light information (incoming photon rate changes). R1-R6 axon terminals then transmit these signals to the lamina network through sign-inverting (histaminergic) output synapses (to L1-L3 monopolar cells and amacrine cells) and receive synaptic feedback (network modulation) in return (Meinertzhagen and O'Neil, 1991; Rivera-Alba et al., 2011); the schematic highlights excitatory feedbacks from L2, lamina intrinsic amacrine neurons (Lai) and L4 to photoreceptor terminals. Because R1-R6s are short and have large length constants, synaptic feedback also influences their somatic response waveforms (Dau et al., 2016; Zheng et al., 2006).

(C) The average $dSlo^-$, dSK^- , $dSK^-;dSlo^-$ and wild-type responses to 10 ms bright and dim flashes. Their corresponding delay and rise times (≤ 20 ms from the flash onset; light gray area) were similar, suggesting intact light information sampling. But the mutant R1-R6 responses decayed (in light brown area) either faster or slower than the wild-type, suggesting differences in neural tuning.

(D) Mutant and wild-type R1-R6 responses had comparable maximum amplitudes over the tested flash intensity range, resulting in similar $V/\log(I)$ saturation curves.

(E) $dSK^-;dSlo^-$ and dSK^- responses peaked, on average, sooner than the wild-type to all test intensities, with significantly shorter dSK^- values for BG-0.5 ($p = 0.028$) and BG-1 ($p = 0.047$). Conversely, $dSlo^-$ responses peaked later than the wild-type to all but the two brightest flashes. Moreover, these responses peaked significantly later than those of dSK^- at BG-0.5 ($p = 0.035$) and BG-3 ($p = 0.013$), and $dSK^-;dSlo^-$ at

BG-2 ($p = 0.038$) and BG-3 ($p = 0.013$).

(F) Wild-type response half-widths to the brightest flash (BG0) were significantly longer than those of dSK^- ($p = 0.003$) and $dSK^-; dSlo^-$ ($p = 8.56 \times 10^{-4}$) R1-R6s. Conversely, $dSlo^-$ responses, on average, lasted the longest over a broad flash intensity range; vs. $dSK^-; dSlo^-$: at BG-1 ($p = 0.042$) BG-2 ($p = 0.011$) and BG-3 ($p = 0.007$).

D-F: Mean \pm SEM, two-tailed t-test.

Response Differences not from Homeostatic Ion Channel Expression

If a R1-R6 photoreceptor was an isolated system, missing Ca^{2+} -activated K^+ -conductances would directly increase its membrane resistance, R_m , and consequently its time constant ($\tau_m = R_m \cdot C_m$; C_m is membrane capacitance). This would slow down voltage responses to light changes. However, *in vivo*, as each R1-R6 features complex bioelectric interactions within its membrane and with its neural neighbors, the mutant responses showed far more sophisticated dynamics (Figure 1), presumably reflecting homeostatic changes in these interactions (Marder and Goaillard, 2006; Vähäsöyrinki et al., 2006). Therefore, to work out what made the mutant R1-R6 outputs differ, we analyzed changes both in their intrinsic (membrane) properties and extrinsic (synaptic) feedback from the surrounding network.

We first asked whether the differences in $dSlo^-$, dSK^- and $dSK^-; dSlo^-$ R1-R6 voltage responses resulted from homeostatic somatic conductance changes. These would affect their membrane resistances, accelerating or decelerating signal conduction. For example, missing dSK channels in dSK^- photoreceptors could be compensated by up-regulating $dSlo$ channel expression, for which these cells carry a normal gene; and *vice versa* in $dSlo^-$ photoreceptors. Alternatively, the cells could increase K^+ - or Cl^- -leak-conductances (Niven et al., 2003; Vähäsöyrinki et al., 2006). While such intrinsic homeostatic mechanisms could accelerate dSK^- R1-R6 output, these would also lower their resting potentials; by reducing depolarizing Ca^{2+} -load and/or increasing hyperpolarizing K^+/Cl^- loads. Equally, a lack of such homeostatic ion channel expression changes could have contributed to $dSlo^-$ photoreceptors' slower signaling.

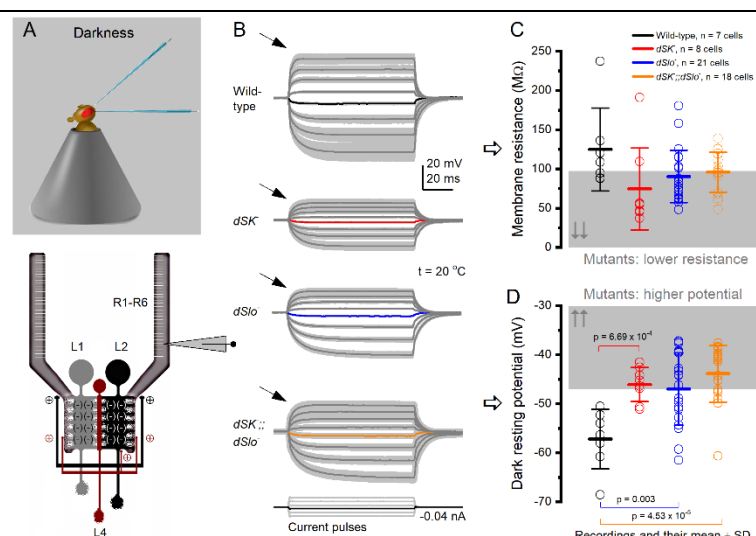


Figure 2. In Darkness, R1-R6 Photoreceptors of Ca^{2+} -Activated K^+ Channel Null-Mutants Have Lower Membrane Resistances and Higher Resting Potentials

(A) *In vivo* R1-R6 recordings. R1-R6 terminals provide histaminergic feedforward inhibition to LMCs. In return, R1-R6s receive excitatory feedback from L2 and L4 monopolar cells.

(B) Voltage responses of dark-adapted wild-type and mutant R1-R6s to intracellular current pulse injections. The

arrows indicate outward rectification; caused by voltage-sensitive Shaker and Shab K^+ -conductance activation to fast membrane depolarizations.

(C) Mean wild-type R1-R6 input resistance (124.8 ± 52.7 MΩ, $n = 7$ cells) is significantly higher than that for all the mutant recordings (89.8 ± 34.5 MΩ, $n = 47$, $p = 0.024$), but not quite for each mutant-type separately

(*dSK*⁻, 74.6 ± 52.0 MΩ, p = 0.087, n = 8; *dSlo*⁻, 90.4 ± 33.4 MΩ, p = 0.052, n = 21; *dSK*⁻;*dSlo*⁻, 95.9 ± 25.6 MΩ, p = 0.074, n = 18).

(D) Mutant R1-R6s are more depolarized than the wild-type photoreceptors in darkness (wild-type, -57.2 ± 6.1 mV; *dSK*⁻, -46.1 ± 3.5 mV; *dSlo*⁻, -47.0 ± 7.4 mV; *dSK*⁻;*dSlo*⁻, -43.9 ± 5.8 mV).

C-D: Mean ± SD, two-tailed t-test.

To test these hypotheses, we measured *in vivo* somatic electrical membrane properties in dark-adapted mutant and wild-type R1-R6s (Figure 2A) using single-electrode current-clamp (e.g. Juusola and Weckström, 1993). We found that all the mutant R1-R6s charged smaller, but broadly wild-type-like voltage responses to injected current pulses (Figure 2B). Depolarization to positive currents showed characteristic outward rectification (arrows), caused by activation of voltage-dependent K⁺ channels (Hardie, 1991a; Hardie et al., 1991; Juusola and Hardie, 2001a; Vähäsöyrinki et al., 2006), while hyperpolarization to negative currents, in effect, charged their membranes passively.

The membrane input resistances of the mutant R1-R6s (Figure 2C), as determined by small hyperpolarizing responses to -0.02 nA current steps, were characteristically lower than in the wild-type (Juusola and Hardie, 2001a; Niven et al., 2003), with the mean resistance of *dSK*⁻ R1-R6s being the lowest (cf. Abou Tayoun et al., 2011). Most crucially, however, the mutant (*dSK*⁻, *dSlo*⁻ and *dSK*⁻;*dSlo*⁻) photoreceptors' resting potentials (Figure 2D), instead of being more hyperpolarized, were >10 mV more depolarized than the wild-type. Here, if *dSK*⁻ or *dSlo*⁻ R1-R6s' intrinsic signaling properties were regulated homeostatically, by ion channel expression (as hypothesized), then their resting potential in darkness should have been below the wild-type range, rather than above it. Also, the higher resting potentials (Figure 2D) and lower membrane resistances (Figure 2C) should have accelerated signal conduction. Yet, the mean *dSlo*⁻ R1-R6 voltage response time-to-peak values to intermediate light flash intensities were, in fact, slower than in the wild-type (Figures 1E and 1F).

Hence, collectively, these results suggested that the accelerated (*dSK*⁻ and *dSK*⁻;*dSlo*⁻) and decelerated (*dSlo*⁻) light-induced voltage response dynamics of the mutant photoreceptors (Figures 1B and 1C) unlikely resulted from compensatory expression of leak- or Ca²⁺-activated K⁺ channels at the somata, but required other/further mechanisms.

Response Differences not by Transduction or K⁺ Conductance Differences

To eliminate the possibility that developmental morphological defects in the mutant R1-R6s would have caused their altered responses, we assessed the mutant and wild-type eyes/retinae using both electron- (Figure 3A, above) and light-microscopy (below). We found no obvious morphological differences between the eyes; with each method displaying highly ordered ommatidia with normal looking intact R1-R7 photoreceptor rhabdomeres.

Nevertheless, deletion of *dSlo*, *dSK* or both could still affect intracellular [Ca²⁺] regulation, and thus potentially alter microvillar phototransduction functions indirectly (Hardie and Juusola, 2015; Song et al., 2012), modifying sampling, amplification or integration of light-induced currents (LIC). We, therefore, used whole-cell recordings in dissociated ommatidia (Hardie, 1991b) (Figure 3B) to compare the mutant and wild-type R1-R6s' elementary responses (quantum bumps, QBs) to single photons (Figure 3C) and macroscopic LICs to light pulses (Figures 3D and 3E). In this preparation, photoreceptor axon terminals were severed, cutting off any synaptic feedback from the lamina network to R1-R6s (Zheng et al., 2006).

1

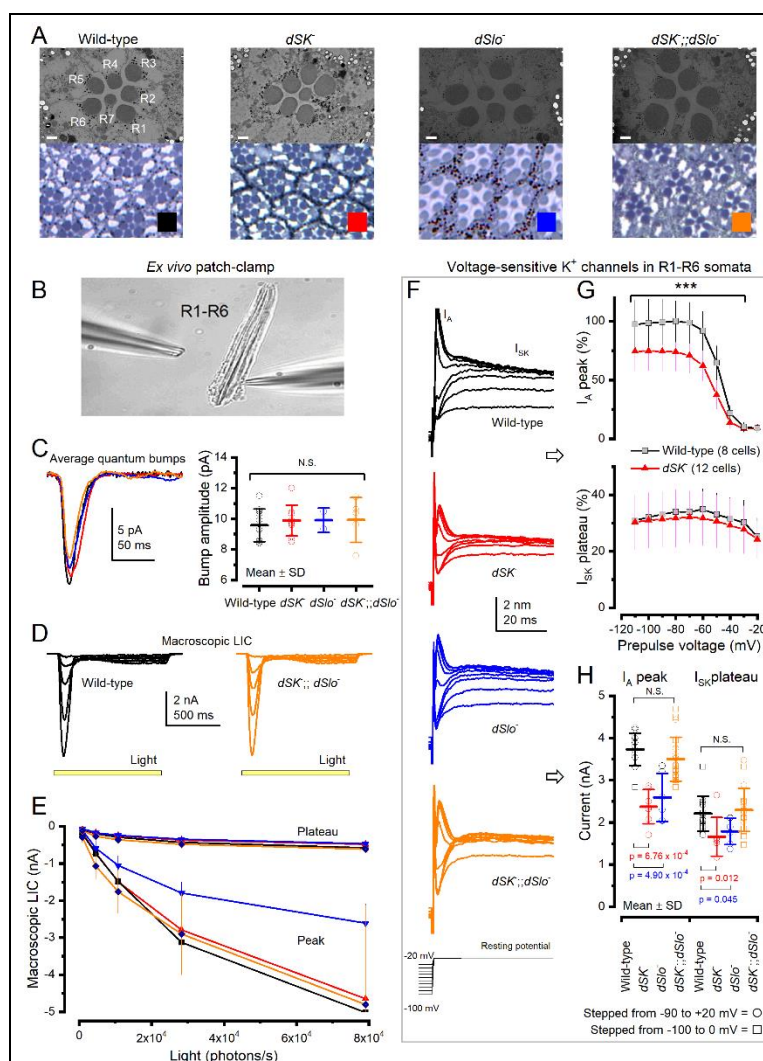


Figure 3. *dSK*, *dSlo* and *dSK;;dSlo* Photoreceptors Have Normal Morphology, Light-Induced Currents (LIC) but 8-40% Reduced Light-Insensitive *I_A* Currents

(A) The mutant retinæ appear structurally intact, with R1-R7s having wild-type-like rhabdomeres and pigmentation; 1 μ m EM scale bars.

(B) Whole-cell recordings were performed from dissociated ommatidia.

(C) Mutant and wild-type R1-R6 quantum bump (QB) waveforms and their amplitude distributions to dim flashes are similar.

(D) Wild-type and *dSK;;dSlo* R1-R6 LIC responses to 1 s light pulses of different brightness.

(E) Macroscopic LIC peak and plateau responses were similar, with the normal experimental variation, indicating that *dSK* and *dSlo* deletions do not affect phototransduction. The smaller *dSlo* max LIC probably resulted from these ommatidia being smaller, reflecting *dSlo* mutants reduced yield/health.

(F) Wild-type and mutant R1-R6s' voltage-sensitive outward K⁺ currents to increased voltage steps contain both the transient Shaker (*I_A*) and sustained delayed rectifier, Shab, (*I_{KS}*) components.

(G) *dSK* R1-R6 K⁺-currents have a reduced *I_A* but near normal-sized *I_{KS}*.

(H) On average, the maximum *I_A* and *I_{KS}* currents in *dSK* and *dSlo* R1-R6s are a bit smaller than the wild-type (*dSK* *I_A*: 36.4% < wild-type, *I_{KS}*: 24.9% < wild-type; *dSlo* *I_A*: 30.6% < wild-type, *I_{KS}*: 19.0% < wild-type) but wild-type-like in *dSK;;dSlo* R1-R6s.

2

3 We found the mutant R1-R6s' bump amplitudes and waveforms (Figure 3C) and macroscopic LICs
4 (Figures 3D and 3E) to increasing light intensities wild-type-like, showing normal dynamics within
5 the normal experimental variation. Here, the smaller *dSlo* LIC maxima likely resulted from the
6 smaller size of these homozygotic mutant flies due to their lower yield/reduced health. Thus, deletion
7 of *dSlo*, *dSK* or both channels neither disrupted the microvillar R1-R6 morphology nor its
8 phototransduction functions, again suggesting that the mutant R1-R6s would sample light
9 information like their wild-type counterparts (see: Hardie and Juusola, 2015; Juusola and Song, 2017;
10 Song et al., 2012).

11

12 Intriguingly, however, K⁺ conductances in dissociated *dSK* and *dSlo* R1-R6s showed slightly
13 reduced (19-36%) fast A- (*I_A* or Shaker) and delayed rectifier currents (*I_{KS}* or Shab) (Figures 3F-H),
14 while these currents were broadly wild-type-like in *dSK;;dSlo* R1-R6s. The decrease in the *I_A* and

I_{KS} currents together with dSK or dSlo current removal should, with other things being equal, increase membrane resistance and its time constant, leading to slower voltage responses. Instead *in vivo*, we found resistance in all the mutant R1-R6s below the wild-type (Figure 2C), with both dSK^- and $dSK^-;dSlo^-$ R1-R6s responding faster and only $dSlo^-$ R1-R6s slower (Figure 1E), implying that homeostatic changes in K^+ channel expression alone cannot explain their response differences.

Together, the observed normal rhabdomere morphology, wild-type-like LIC dynamics and only partly reduced photo-insensitive membrane conductances implied that the mutant R1-R6s' accelerated or decelerated voltage responses, higher resting potentials and lower membrane resistance *in vivo* could not be induced by homeostatic ion channel expression changes in photoreceptor somata alone. But this would more require network adaptation (Nikolaev et al., 2009; Zheng et al., 2009), parallel changes in the synaptic network activity. In such scenarios, missing one or both Ca^{2+} -activated K^+ channels would cause a homeostatic (automatic) rebalancing of the bidirectional signal transfer between photoreceptor axon terminals and the lamina interneurons (Abou Tayoun et al., 2011; Dau et al., 2016; Shaw, 1984; Zheng et al., 2006; Zheng et al., 2009).

dSK or dSlo Absence Changes Network Adaptation

In the adult *Drosophila* brain, dSlo and dSK share similar expression patterns with higher expression in the lamina and medulla neuropils and weaker in the retina (Abou Tayoun et al., 2011; Becker et al., 1995). Thus, theoretically, dSlo and dSK could co-participate in shaping the bidirectional signal transfer between R1-R6 photoreceptor axons and LMCs, which form columnar R-LMC-R network processing units in the lamina (Nikolaev et al., 2009; Zheng et al., 2009). Here, the deletion of one or the other ion channel could disrupt this balance.

We, therefore, next asked how Ca^{2+} -activated K^+ channels might contribute to network adaptation in the R-LMC-R system. We recorded dSK^- , $dSlo^-$, $dSK^-;dSlo^-$ and wild-type R1-R6 responses to a repeated 1 s naturalistic light intensity time series stimulus (NS) (van Hateren, 1997) *in vivo*, and found each of them adapting differently (Figure 4A).

The mean of the wild-type response (Figure 4B, black trace; measured at each second) decreased approximately exponentially as the cells adapted to NS (Figure 4C), reaching a relative steady-state in 15-20 s (Figures 4B and 4C). In contrast, the corresponding means of the mutant responses declined faster but then displayed unique genotype-specific undershooting. The means of dSK^- (red trace) and $dSK^-;dSlo^-$ (orange) responses first decreased to their minima in <10 s, and then increased, as the cells gradually further depolarized, reaching a relative steady-state in 35-40 s; ~20 s later than the wild-type. While the mean of $dSlo^-$ photoreceptor output (blue) decayed slower than in the other mutant R1-R6s and undershot less.

Concurrently, the wild-type and mutant R1-R6 output ranges - measured as the standard deviation (Figure 4D) of their response waveforms (Figure 4C) at each second of NS - adapted with distinctive dynamics and speeds. $dSlo^-$ R1-R6 outputs desensitized the slowest, slower than the wild-type, with their ranges compressing with different average time courses ($T_{dSlo^-} = 3.41 \pm 3.28$ s, $n = 19$ cells [22 recordings]; $T_{wild-type} = 1.47 \pm 0.67$, $n = 7$ cells [10 recordings]; mean \pm SD) (Figure 4D). Conversely, dSK^- and $dSK^-;dSlo^-$ R1-R6 output ranges first compressed as rapidly as the wild-type ($T_{dSK^-} = 1.45 \pm 0.66$, $n = 7$ cells [7 recordings]; $T_{dSK^-;dSlo^-} = 1.44 \pm 0.32$, $n = 8$ cells [9 recordings]), but then slowly begun to expand, reflecting their rather similar mean voltage dynamics (Figure 4B). The adaptive

range reduction occurred most severely in $dSK^{+/-};dSlo^{-}$ and $dSlo^{-}$ R1-R6s, leaving their steady-state responses ~10% smaller than those of the wild-type.

These results highlight the complex role of Ca^{2+} -activated K^{+} channels in regulating R1-R6 output in network adaptation. While the absence of dSlo channel slowed adaptation in $dSlo^{-}$ R1-R6s, the dSK^{-} and the double-mutant $dSK^{+/-};dSlo^{-}$ R1-R6s adapted faster but showed overshooting dynamics. Consequently, as an overall sign of compromised gain control, the mutant R1-R6s reached their steady-state responsiveness 20-30 s later than the wild-type. Thus, each mutant R-LMC-R system adapted suboptimally, constrained to its own unique dynamics.

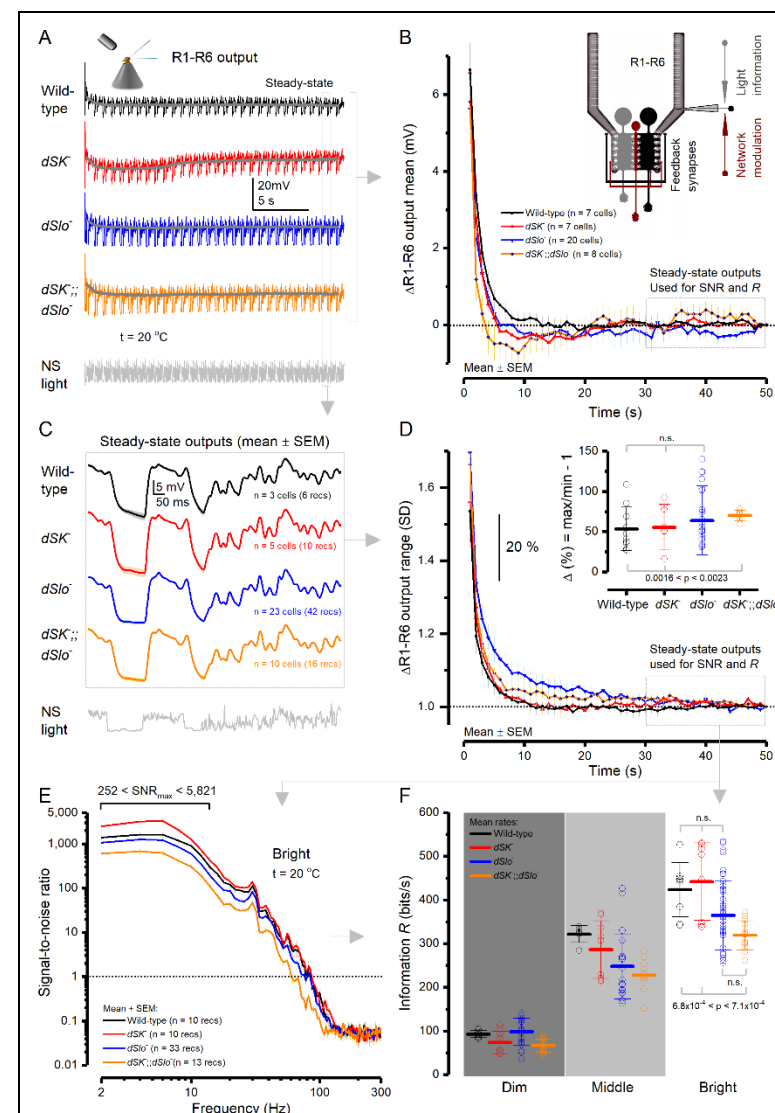


Figure 4. Adaptation Dynamics and Information Rates of Wild-Type and Ca^{2+} -Activated K^{+} Channel Null-Mutant R1-R6 Photoreceptors

(A) Intracellular voltage responses to a repeated 1-s-long bright naturalistic light intensity time series stimulus (NS).

(B) Change in the response mean (± SD) over the repeated stimulation. Mean wild-type and $dSlo^{-}$ R1-R6 outputs declined near exponentially to steady-state, whereas adaptation in mean dSK^{-} and $dSK^{+/-};dSlo^{-}$ R1-R6 outputs depicted unique undershoots.

(C) Mean waveforms ± SD of steady-state adapted 1 s responses.

(D) Relative change in R1-R6 output range, measured as the standard deviation (SD) of the responses at each s during 50 s of stimulation (mean ± SD). Wild-type and $dSlo^{-}$ R1-R6s desensitized during repeated stimulation, following exponential time constants. Wild-type R1-R6 output range contracted from 114% to 100% in about 26 s ($\tau_{\text{Wild-type}} = 1.96 \pm 0.39$ s); $dSlo^{-}$ from 134% in about 19 s ($\tau_{dSlo4} = 8.3 \pm 1$ s); $dSK^{+/-};dSlo^{-}$ from 133% in 8 s ($\tau_{dSK^{+/-};dSlo4} = 3.4 \pm 0.4$ s). dSK^{-} and $dSK^{+/-};dSlo^{-}$ R1-R6s' output ranges showed further sensitizing trends, reaching a steady-state after ~40 s.

(E) Mutant and wild-type R1-R6s' average signal-to-noise ratios, measured from their steady-state outputs to bright NS, are high and broadly similar.

(F) Mutant and wild-type R1-R6s sampled information from dim, moderately intense (middle) and bright naturalistic stimulation in a comparable manner (mean ± SD; n = 10-33 recordings). $dSK^{+/-};dSlo^{-}$ R1-R6s had a marginally lower mean information transfer rate than the other genotype photoreceptors. In each genotype, R1-R6 information rates to the given stimulation vary naturally (up to ~200 bits/s) as each cell receives different amount of information from the network (Juusola et al., 2017).

dSK or dSlo Absence Leaves Information Sampling Intact

A R1-R6's information transfer rate depends mostly on its photon-absorption rate changes, set by the number of individual sampling units (rhabdomeric microvilli) and the speed and refractoriness of their phototransduction reactions (Juusola et al., 2017; Juusola and Song, 2017; Song et al., 2012). In contrast, obeying the data processing theorem, any changes in membrane filtering affect signal and noise equally, and therefore cannot increase information (Cover and Thomas, 2006; Juusola and de Polavieja, 2003; Shannon, 1948). Accordingly, information transfer rates of mutant photoreceptors with normal phototransduction but without specific K^+ channels, such as the slow delayed rectifier Shab (I_{KS}) (Vähäsöyrinki et al., 2006), are broadly wild-type-like. But mutations that damage ion channels can destroy information. For example, *Sh* mutant R1-R6s' "nonfunctional" Shaker (I_A) K^+ channels appears to truncate signal amplification while generating noise, reducing information flow (Niven et al., 2003). Critically, however, the R-LMC-R system has intrinsic potential to combat detrimental changes within its parts. A R1-R6's impaired function can be compensated in part by extra light information (through gap-junctions and feedback synapses) from its neighbors, in which receptive fields face the same visual area (Juusola et al., 2017; Shaw, 1984; Wardill et al., 2012; Zheng et al., 2006).

Because *dSlo*⁻, *dSK*⁻ and *dSK*⁻;*dSlo*⁻ mutant R1-R6s lack completely their functional channels (which thus should not generate extra noise) and have normal rhabdomere morphology and LIC dynamics (Figure 3), theoretically, their somatic information transfer rates should be wild-type-like, or slightly lower; in case, their LMC feedback was compromised.

To test this hypothesis, we compared *dSlo*⁻, *dSK*⁻ and *dSK*⁻;*dSlo*⁻ R1-R6s' encoding performance to the wild-type control using the same recordings as above. In each case, the first 20-30 responses with the adapting trends were removed. The signal was taken as the average of the next 20 responses, which thus had settled to a relative steady-state, with its power spectrum calculated by Fourier transform. The corresponding noise power spectrum was estimated from the difference between each response and the signal (see STAR Methods).

We found that the mutant R1-R6s' signal-to-noise ratios (Figure 4E) and information rates (Figure 4F) were broadly wild-type-like; increasing in parallel with brightening light, as tested for dim, middle and bright NS. Thus, as hypothesized, after the initial ~20-30 s adaptation phase, the loss of dSK, dSlo or both channels affected only marginally a R1-R6's encoding performance. These results highlight the R-LMC-R system's robustness and compensatory ability to withstand internal damage.

dSK or dSlo Absence Increases Synaptic Feedback

To work out in theory how synaptic feedback from the lamina interneurons should shape the wild-type R1-R6 output and how homeostatic feedback changes should shape mutant R1-R6 outputs, we next combined biophysical R1-R6 modelling with intracellular recordings.

Our biophysical R1-R6 model (Figure 5A) incorporates 30,000 computational microvilli (Song et al., 2012), each of which implements full stochastic phototransduction reactions to transduce absorbed photons into QBs. Essentially, this model samples light information much like a real R1-R6 (Juusola et al., 2017; Juusola and Song, 2017; Song and Juusola, 2014; Song et al., 2012). Its QBs sum up realistic macroscopic LIC, with the best performance for naturalistic stimuli at $1-8 \times 10^5$ photon

absorptions/s (Juusola et al., 2017; Song and Juusola, 2014). LIC then charges a Hodgkin-Huxley-type photoreceptor membrane circuit (Figure 5B; see also Figure 3) (Niven et al., 2003; Song and Juusola, 2014; Song et al., 2012; Vähäsöyrinki et al., 2006), generating output that approximates intracellular recordings to comparable light stimulation (Juusola et al., 2017; Song and Juusola, 2014, 2017; Song et al., 2012). Most differences in the simulated and recorded response waveforms would then be caused by the real R1-R6s' synaptic feedback currents - input from LMCs (Dau et al., 2016; Rivera-Alba et al., 2011; Zheng et al., 2006), which the model lacks (Juusola et al., 2017). Moreover, given that the mutant R1-R6s' phototransduction is wild-type-like and voltage-sensitive conductances either wild-type-like or only moderately reduced (Figure 3), their voltage response differences should also mostly reflect synaptic feedback differences (Figure 4).

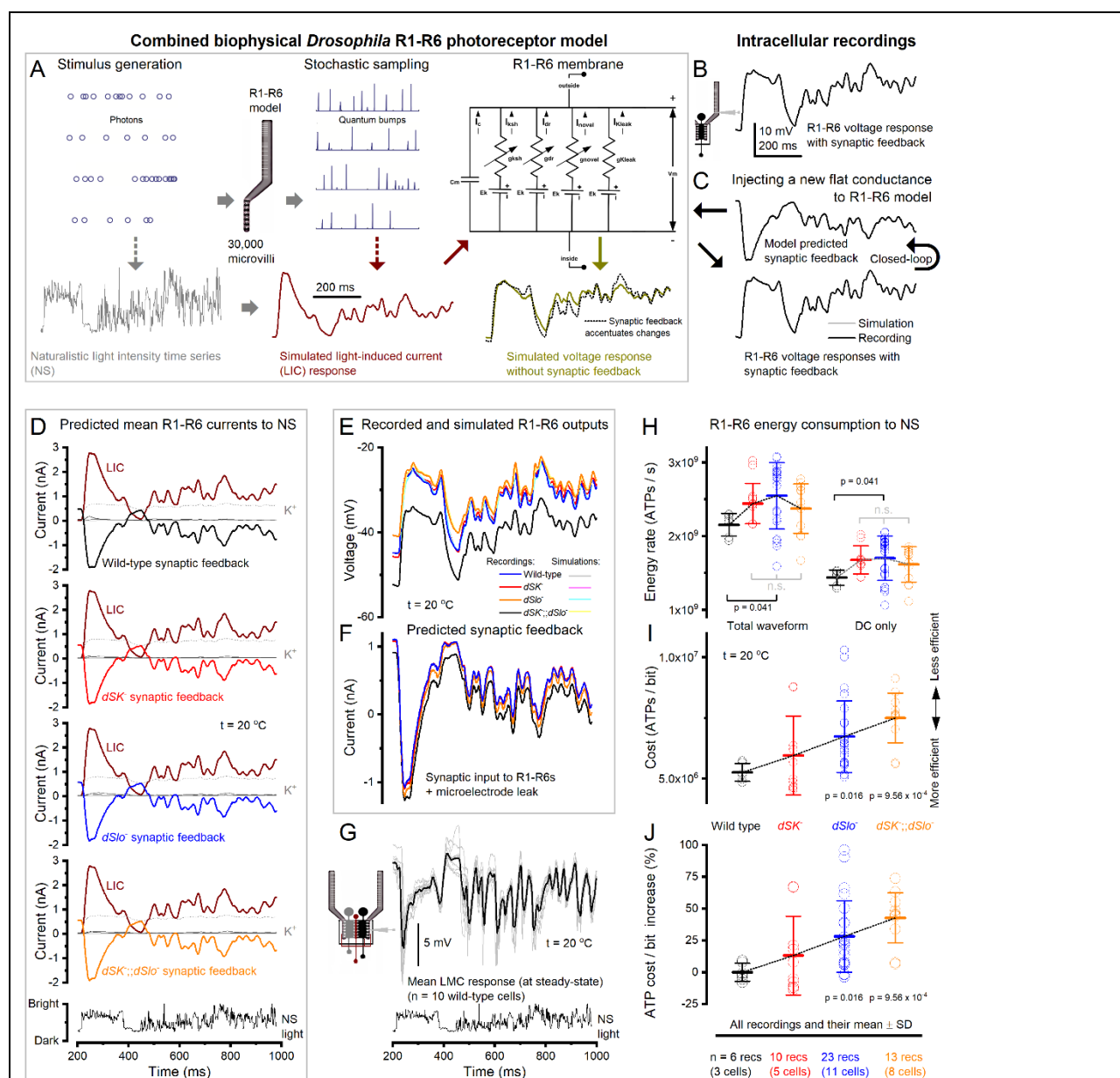


Figure 5. Predicted Synaptic Feedback and ATP Consumption of Wild-Type and Mutant R1-R6 Photoreceptors

(A) Biophysically realistic R1-R6 model has four modules: stimulus generation, stochastic photon sampling/quantum bump generation, bump integration and voltage-sensitive membrane. But it lacks the synaptic feedback from the lamina network (Juusola et al., 2017; Song and Juusola, 2017), which affect the

real R1-R6 output. R1-R6 simulations (dark yellow trace) and recordings (dotted trace) to a repeated naturalistic light intensity time series (NS) were analyzed at relative steady-state adaptation (cf. [Figure 4C](#)).

(B) Characteristic recording waveform to bright NS (BG0).

(C) Synaptic feedback to each recording was estimated computationally by linking it to the photoreceptor model, which had no free parameters. A new flat (zero) conductance, representing the synaptic input, was then injected to the model. This conductance waveform was shaped in a closed-loop until the model output (gray) matched the recorded output (black).

(D) The fixed light-induced (dark red), K^+ currents and the average predicted synaptic feedback and of wild-type and mutant R1-R6 recordings.

(E) Together, these currents charged up their respective simulated R1-R6 voltage responses. The simulations (light colors) match the recordings (bright colors) near perfectly.

(F) The average predicted synaptic feedback was unique to the mutant R1-R6s and showed stronger modulation on a higher mean (tonic excitatory background) than the wild-type (see also [Figure S3F](#)). Testing the feedback means across all recordings: wild-type vs dSK^- , $p = 0.041$; dSK^- vs $dSlo^-$, $p = 0.033$; $dSlo^-$ vs $dSK^-; dSlo^-$, $p = 0.009$; testing the mean feedback waveforms against each other, $p < 2.274 \times 10^{-62}$.

(G) Separately recorded large monopolar cell (LMC) response waveforms to the same NS much resemble the predicted feedback waveforms (in F), suggesting that L2 and L4 cells, which form feedback synapses with R1-R6s ([Meinertzhagen and O'Neil, 1991](#); [Rivera-Alba et al., 2011](#)), would contribute to R1-R6 output modulation ([Zheng et al., 2006](#)).

(H) With these conductances included in each separate wild-type, dSK^- , $dSlo^-$ and $dSK^-; dSlo^-$ R1-R6 models, the metabolic energy (ATP) consumption of each recording was calculated for its full waveform (left) ([Song and Juusola, 2014](#)) and DC voltage (right) ([Laughlin et al., 1998](#)), respectively. Notably, the original DC voltage method, which does not consider how the dynamic ion fluctuations add to the electrochemical pumping work, underestimates ATP consumption by 1/3 (33.2%; see STAR Methods).

(I) The cost of neural information, was calculated for each recording by dividing its information rate estimate with its full ATP consumption rate estimate. On average, the absence of dSK or $dSlo$ or both increased the cost of neural information in a mutant R1-R6 by 13.1% (dSK^-), 28.0% ($dSlo^-$) or 42.7% ($dSK^-; dSlo^-$).

Therefore, we could extrapolate the synaptic feedback current to each recorded R1-R6, whether wild-type or mutant, computationally ([Figure 5C](#)) by using the same fixed LIC with their specific I_A and I_{SK} current dynamics ([Figure 3](#) and [S1](#)). In these simulations, we first injected a new flat (zero) conductance, representing the missing synaptic input, to the full R1-R6 model. The software then shaped up this conductance waveform in a closed-loop until the model's voltage response matched the recorded response for the same light stimulus. Thus, theoretically, the resulting (predicted) current should closely mimic the real synaptic feedback, which the tested R1-R6 would have received from the lamina network *in vivo*.

[Figure 5D](#) shows the corresponding mean LIC and synaptic feedback estimates to repeated light stimulation for the tested wild-type and mutant photoreceptors, and the concurrent voltage-sensitive K^+ currents and K^+ leak estimates. In these simulations, whilst the LIC was the same (fixed; dark red traces) for every genotype, their synaptic feedback and K^+ (dark green) currents balanced out differently to reproduce their respective *in vivo* voltage signals ([Figure 5E](#)).

We found that in every simulation the predicted synaptic feedback to R1-R6s was excitatory, graded and phasic ([Figures 5D](#) and [5F](#)). It rapidly increased ("switched-on") during light decrements and decreased ("switched-off") during light increments. This accentuated transient (phasic) light changes

in photoreceptor output (Figure 5E; cf. 5A). Moreover, the predicted synaptic excitatory load to R1-R6s (Figure 5F) was unique for each mutant and the wild-type flies with the highest mean to dSK^- (red) and $dSlo^-$ (blue) photoreceptors. Thus, the enhanced excitatory feedback conductance from the lamina interneurons is the most probable mechanistic explanation of why and how the mutant photoreceptors were more depolarized than their wild-type counterparts, both in darkness (cf. Figure 2D) and during light stimulation (Figure 5E).

Remarkably, these feedback dynamics (Figure 5F), which were extrapolated using only photoreceptor data (Figures 5A-C), closely resembled postsynaptic intracellular LMC responses to the same light stimulus (Figure 5G). This implied that L2, L4 and lamina intrinsic amacrine neurons (Lai), all of which receive inhibitory inputs from R1-R6 but form excitatory feedback synapses to R1-R6 (Hu et al., 2015; Kolodziejczyk et al., 2008; Raghu and Borst, 2011), could alone or together be the major source of this feedback. Thus, these new findings are consistent with our theory of how the R-LMC-R system, by dynamically balancing its inhibitory and excitatory synaptic loads, shapes the early neural representation of visual information (Dau et al., 2016; Nikolaev et al., 2009; Zheng et al., 2006; Zheng et al., 2009).

dSK and dSlo Lower Neural Information Energy Cost

In response to LIC and synaptic feedback, ion channels open and close, regulating the ionic flow across the photoreceptor membrane. Meanwhile its ion cotransporters, exchangers and pumps uptake or expel ions to maintain ionic concentrations in- and outside. The work of the pumps in moving ions against their electrochemical gradients consumes ATP (Laughlin et al., 1998). For a R1-R6, a reasonable estimate of this consumption can be calculated from the ionic flow dynamics through its ion channels; details in STAR Methods (see also: Song and Juusola, 2014).

Using our biophysical R1-R6 model, which now included the synaptic feedback, we calculated how much each recorded wild-type and mutant R1-R6 consumed metabolic energy (ATP molecules/s) to encode bright naturalistic light changes (Figure 5H, left). We discovered that because their enhanced synaptic feedback held dSK^- , $dSlo^-$ and $dSK^-;dSlo^-$ R1-R6s at higher operating voltages, where signaling is more expensive, they consumed on average 13.3%, 18.3% and 10.2% more ATP than the wild-type, respectively.

We also estimated each tested R1-R6's ATP consumption by using the method of balancing out the ionic currents for its light-induced mean (flat) depolarization level, or DC (Laughlin et al., 1998). This produced a metric, which followed quite a similar trend (Figure 5H, right). But because it discarded how much the dynamic ion fluctuations increase the work to maintain transmembrane ionic concentration, it underestimated the total ATP consumption by $\sim 1/3$.

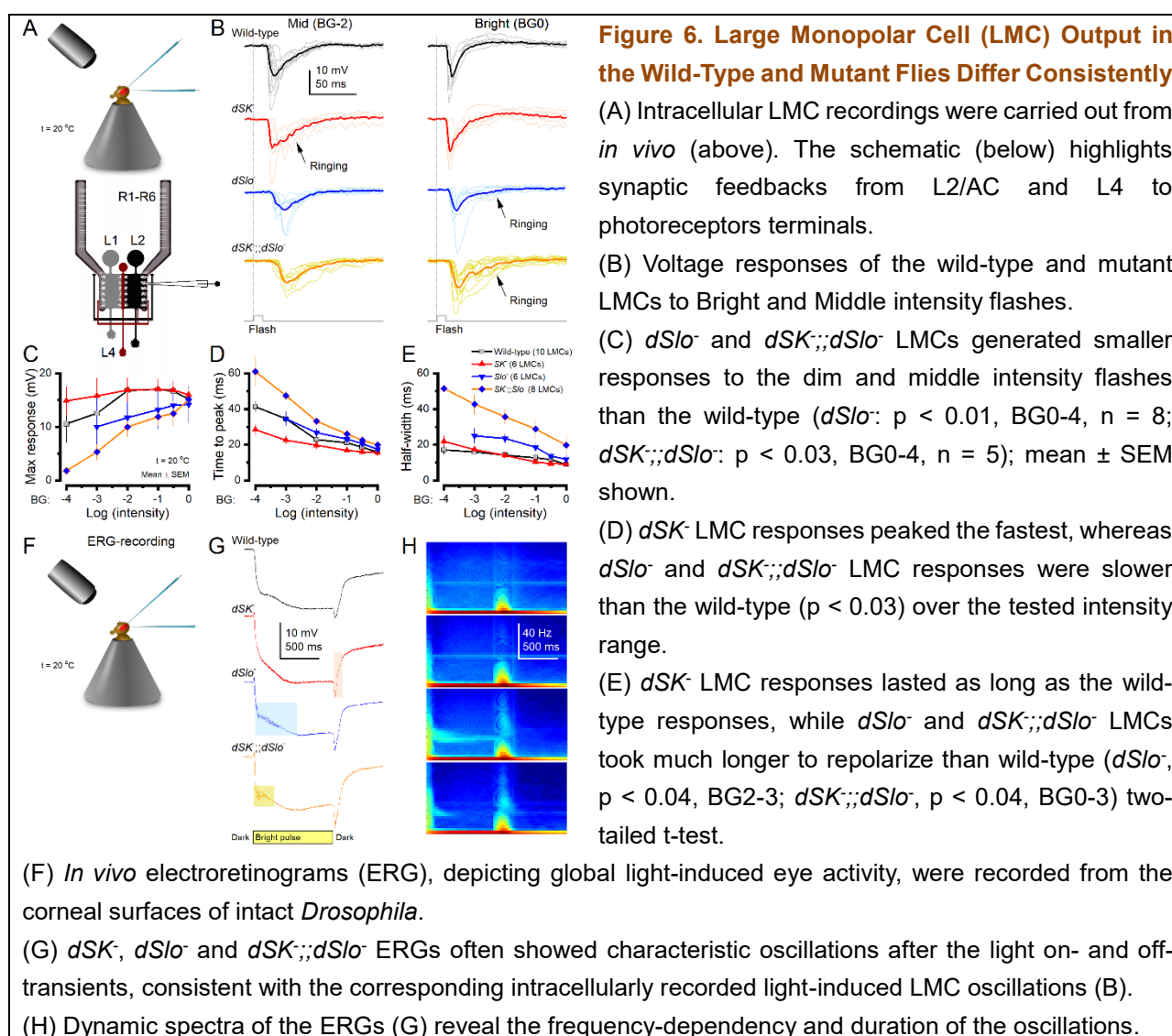
Next, using the full biophysical models, we calculated how the mutant R1-R6s' homeostatically reduced *Shaker* and *Shab* K^+ conductances (Figures 3F-H) affect their neural information costs (Figure S2). We fixed the *Shaker* and *Shab* conductance dynamics of the dSK^- , $dSlo^-$ and $dSK^-;dSlo^-$ R1-R6 models to match typical wild-type R1-R6 VC-recordings (Figure S1A). This increased the mutant photoreceptors' energy consumption, but only slightly (Figure S2H). Hence, the observed homeostatic 19-36% *Shaker* and *Shab* current reduction in dSK^- and $dSlo^-$ R1-R6s (Figures 3F and 3H) made evolutionary sense, as it cut both their hyperpolarizing drive, which therefore would require less excitatory synaptic feedback to depolarize the cells, and neural information costs. But this saving

was small, only 4.5-6.2%. And somewhat unexpectedly, its homeostatic effect, in fact, increased the dSK^- and $dSlo^-$ R1-R6s' synaptic feedback overload slightly in respect to $dSK^-;;dSlo^-$ R1-R6s, which had wild-type-like *Shaker* and *Shab* conductance dynamics (Figure 5F). Moreover, simulations about other possible homeostatic changes (Figure S3) indicated that by increasing leak and voltage-sensitive K^+ conductances, or adding an extra Cl^- -leak, in the R1-R6 membrane would strengthen and accentuate synaptic feedback (Figure S3F), and by that increase both the wild-type R1-R6s' ATP consumption (Figure S3H; now by 23.2%) and the mutant photoreceptors' neural information costs in respect to the wild-type (Figures S3I and S3J), now by 22.3% (dSK^-), 37.0% ($dSlo^-$) or 57.6% ($dSK^-;;dSlo^-$). Therefore, as energy wasting reduces fitness, the earlier proposed leak-conductance overexpression alone (Niven et al., 2003; Vähäsöyrinki et al., 2006) seems an unlikely homeostatic strategy here.

These results establish the extra energy, which a mutant R1-R6 must spend to function without Ca^{2+} -activated K^+ channels, as a major cost for homeostatic compensation of neural information (Figure 5I). To maintain similar information rates (Figure 4F), an average mutant R1-R6 consumed at least 13.1% (dSK^- ; $p = 0.114$), 28.0% ($dSlo^-$; $p = 0.016$) or 42.7% ($dSK^-;;dSlo^-$; $p = 9.56 \times 10^{-4}$) more ATP for each transmitted bit than its wild-type counterpart (Figure 5J). Notably, these costs would only increase further if homeostatic compensation of the missing dSK and dSlo channels further entailed over-expression of additional K^+ or Cl^- conductances or leaks (Figures S2 and S3). Thus, in *Drosophila* photoreceptors, Ca^{2+} -activated K^+ channels reduce the energy cost of neural information.

dSlo and dSK Co-Regulate Feedforward Transmission to LMCs

Thus far, we have provided experimental and theoretical evidence that both BK ($dSlo$) or dSK channel deletions enhance synaptic feedback from the lamina interneurons to R1-R6s (Figures 1-5). But these results still leave open the corresponding changes in the post-synaptic LMC output, which initiates the motion vision pathways to the fly brain (Joesch et al., 2010; Wardill et al., 2012). To test how dSK and dSlo deletions affect such feedforward transmission directly, we recorded intracellular voltage responses of dark-adapted LMCs in the mutant and wild-type laminae to brightening light flashes, which covered a 4-log intensity range (Figure 6A).



Expectedly, light rapidly hyperpolarized LMCs and darkness depolarized them (Figure 6B) (Juusola et al., 1995; Zettler and Järvilehto, 1973; Zheng et al., 2006), driven by the photoreceptors' inhibitory transmitter, histamine (Dau et al., 2016; Hardie, 1989). Yet, these dynamics varied somewhat systematically between the genotypes, with the mutant LMCs often showing oscillating responses (ringing) around specific frequencies. L1 (on-pathway) and L2 (off-pathway) responses are thought to be largely similar at the dendritic (lamina) level (Hardie and Weckström, 1990; Nikolaev et al., 2009; Uusitalo et al., 1995) (cf. Figure 5G), with their medulla terminals' light-on and -off preference (Freifeld et al., 2013; Joesch et al., 2010) most likely arise through specific medulla circuit processes. Therefore, with most penetrations likely from L1 and L2, which are the largest LMCs, our recordings should mostly depict mutation-induced variations and less LMC-type-dependent differences.

dSK⁻ LMC output was consistently the most transient, even to dim flashes (Figures 6B-E), showing accelerated (most "light-adapted") dynamics with the fastest time-to-peak values (Figure 6D). By and large, the size (Figure 6C) and half-width (Figure 6E) of these responses were wild-type-like, but, unlike the wild-type, they often showed rapid oscillation bursts to dim flashes (see also Abou Tayoun et al., 2011).

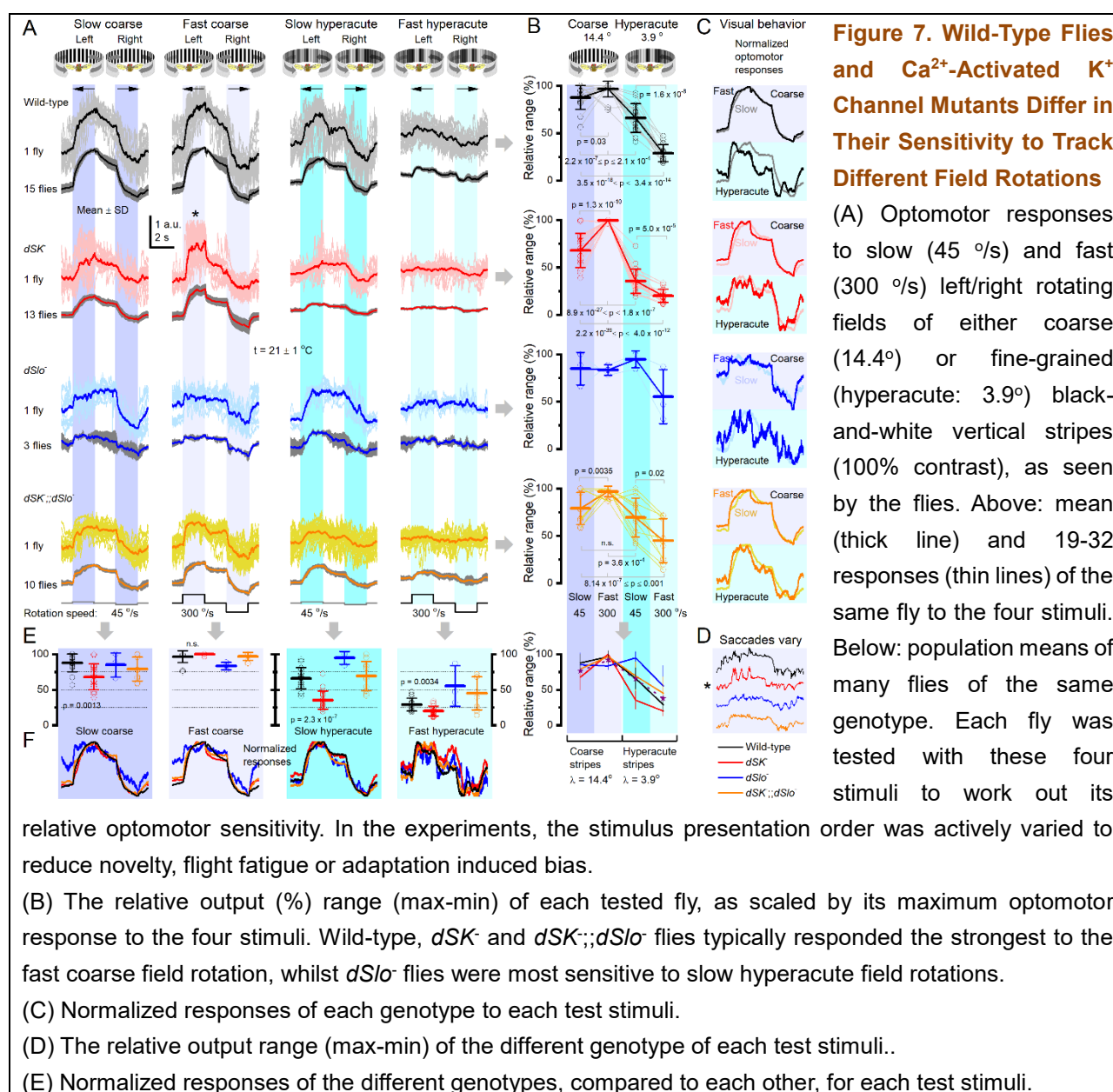
In contrast, both *dSlo*⁻ and *dSK;;dSlo*⁻ LMC responses to dimmer flash intensities were on average

smaller than those of the wild-type and *dSK*⁻ LMCs (Figures 6B and 6C). But as their amplitudes increased with light intensity, the brightest flashes evoked about the same size responses from all the genotypes (Figures 6B and 6C). Therefore, during dim (but not bright) stimulation, the excitatory feedback from L2 and L4 cells to R1-R6s (Zheng et al., 2006) could be driven by smaller *dynamic* modulation on a larger *static* load. This would reduce R1-R6 membrane impedance and, presumably, synaptic gain in R1-R6 output; consistent with the smaller *dSlo*⁻ and *dSK*⁻;*dSlo*⁻ R1-R6 responses to dim naturalistic light stimulation (Figure 4C). Furthermore, *dSK*⁻;*dSlo*⁻ LMC response dynamics were also slower and less tightly time-locked (Figure 6D); often ringing sluggishly (Figure 6B), prolonging the response half-width (Figure 6E) and peaking later than the other corresponding LMC responses (Figure 6D). Such desynchrony would add noise in the synaptic feedback, and may have contributed to the slightly lower signal-to-noise ratios and information transfer rates of *dSK*⁻;*dSlo*⁻ R1-R6s (Figure 4E).

Thus, deletion of *dSK*, *dSlo* or both led to suboptimal network adaptation in the R-LMC system, seen as accelerated or decelerated LMC responses and mutation-specific oscillations. Crucially, these oscillations, with their characteristic frequencies, were also regularly observed in the mutant eyes' global electrical activity (electroretinograms, ERGs) (Figures 6F-H), supporting the intracellular results.

Mutants' Optomotor Responses Reflect Early Vision Defects

To test whether the mutation-specific network adaptations influence visual perception, we measured the flies' optomotor behavior in a classic flight simulator system (Figure 7A). The tethered wild-type and mutant flies generated yaw torque by attempting to follow left and right rotating panoramic scenes, which showed either coarse (14.4°) or fine-grained (3.9°) vertical black-and-white stripe patterns, facing the flies. The resulting optomotor response waveforms and sizes were used to quantify how well individual flies and their respective populations (genotypes) saw these scenes rotating either slowly (45 °/s) or fast (300 °/s). Note that although the average inter-ommatidial angle (the eyes' optical limit) is 4.5° (Gonzalez-Bellido et al., 2011), photomechanical photoreceptor microsaccades enable *Drosophila* to see much finer (hyperacute) details (Juusola et al., 2017).



We found that flies of each genotype could follow these stimuli (Figure 7A), indicating that their visual systems represented and motor systems reacted to the opposing (left and right) image motion appropriately. However, the relative optomotor response sizes (Figure 7B) and waveforms (Figure 7C) showed genotype-specific sensitivities, or stimulus preferences, which were both repeatable and independent of the stimulus presentation order. Thus, these response differences could not be caused by stimulus salience, neural habituation or flight muscle fatigue.

Wild-type flies preferred, on average, the fast coarse stripe field rotations (Figure 7B, black; $96.6 \pm 8.5\%$ maximum response, mean \pm SD, $n = 15$ flies) over the slow coarse ($87.8 \pm 12.6\%$) and slow hyperacute ($66.1 \pm 15.2\%$) stimuli, but only just. Even their responses to fast hyperacute rotations were substantial ($28.9 \pm 9.0\%$), consistent with *Drosophila*'s high visual acuity even at saccadic speeds (>200 °/s) (Juusola et al., 2017). Such an all-round optomotor performance over a broad motion stimulus range implied high early visual system adaptability, providing reliable perception.

In contrast, *dSK*⁻ mutants responded far more strongly to the fast coarse rotating field (Figure 7B,

red; $99.8 \pm 7.6\%$ maximum response, $n = 13$ flies) than the other stimuli (19.9-68.0%), with their slow and fast hyperacute field rotation responses being significantly weaker than those of the other genotypes (Figure 7E). Interestingly and distinctively, the *dSK*⁻ responses were further dominated by large and fast body saccades (* in Figure 7A), which appeared at seemingly regular intervals from the stimulus onset onwards and could make >50% of their total amplitude (Figure 7D). Thus, the accelerated *dSK*⁻ photoreceptor and LMC dynamics (cf. Figures 1C and 6C), and tendency to oscillate, seem preserved in the *dSK*⁻ visual system, with these motion perception distortions possibly compelling their “spiky” optomotor responses.

The optomotor behavior of *dSlo*⁻ mutants showed similarly suggestive correlations to their R-LMC-R network adaptation dynamics. These flies, which boast slightly decelerated photoreceptor (Figure 1E) and LMC (Figure 6D) dynamics, preferred slow field rotations, and, surprisingly, were most sensitive to the slow hyperacute stimulus (Figure 7B, blue; $94.8 \pm 9.0\%$, $n = 3$ flies). Although *dSlo*⁻ mutants, in absolute terms, generated the weakest flight simulator torque responses of the tested genotypes, the mutants that flew did so over the whole experiments, making these stimulus preferences genuine.

Finally, the sensitivity of *dSK*⁻;*dSlo*⁻ mutant responses (Figure 7B, orange) followed the average of *dSK*⁻ and *dSlo*⁻ mutants’ optomotor responses (Figure 7B, purple dotted line) more closely than the mean wild-type responses (black). In particular, their responses were relatively more sensitive to hyperacute stimuli than the corresponding wild-type responses (Figure 7E) but rose and decayed slower (Figure 7F, arrows), consistent with *dSK*⁻;*dSlo*⁻ having slower LMC dynamics (Figures 6D and 6E). Thus, suggestively, their optomotor dynamics differences reflected more differences in early visual network adaptations rather than in other systems, such as the sensorimotor.

DISCUSSION

Our results indicate that *dSlo* (BK) and *dSK* (SK) reduce excitability and energy (ATP) consumption while increasing adaptability and dynamic range for transmitting neural information at the lamina network, ultimately stabilizing visual perception in changing light conditions. Here, single- and double-mutant photoreceptors showed either accelerated or decelerated responses and more depolarized resting potentials during steady-state adaptation. Such changes likely emerged from suboptimal homeostatic rebalancing of synaptic feed-forward and feedback signaling between photoreceptor axon terminals and the rest of the lamina network. Notably, this network compensation was unique for each mutation, resulting in distinctive adaptive regimes; with their respective LMCs showing oscillating accelerated or decelerated responses with reduced output ranges. These altered LMC response dynamics, and thus the flow of visual information, most probably distorted the mutants’ rotating scene perception, and their optomotor responses, in relation to the wild-type.

Homeostatic Compensation Shapes both Electrical Responses and Synaptic Release

Because of the continuous bidirectional adapting interactions between photoreceptors and different lamina interneurons, the altered LMC responses cannot be explained simply by the absence of *dSK* and *dSlo* channels in the LMCs. In blowfly (*Calliphora*) LMCs, Ca^{2+} -activated K^+ channels have been found in low densities in ~20% of perfused inside-out patches (Hardie and Weckström, 1990), suggesting that *dSK* and *dSlo* might be expressed selectively only in certain lamina interneurons. Equally, anti-*dSK* antibody labelling in adult *Drosophila* lamina (Abou Tayoun et al., 2011) implied that *dSK* is absent from L1 and glutamatergic feedback neurons, L2 and Lai, while expressed in R1-

R6 axons and L4 neuron, which makes lateral cholinergic feedback connections into R1-R6 axons and L2 (Kolodziejczyk et al., 2008). Here, missing dSK would alter L4 response dynamics, and by that its synaptic feedback to R1-R6 axons and L2, and from there, L2 feedback to R1-R6. These changes would further reshape the already altered electrical response waveforms of *dSK*⁻ R1-R6s and their histaminergic input to LMCs, resulting in uniquely adapted LMC response dynamics. So, the homeostatic changes in the R-LMC-R system should involve both R1-R6s' and LMCs' electrical response waveforms and their synaptic release machineries. In support of our theory, the electrical response waveforms of LMCs (Figure 6B), which should consist mostly L1 and L2 monopolar cells that lack dSK channels, were different in *dSK*⁻ and wild-type flies; with *dSK*⁻ LMC waveforms peaking faster (Figure 6D) and often oscillating to dim light.

Ca²⁺-activated K⁺ Channels Reduce Costs of Adaptation and Increase Its Range

Adaptability is critical for animal fitness. In sampling and transmission of sensory signals, it reduces communication errors, such as noise and saturation, by continuously adjusting new responses by the memories of the past stimuli (Juusola and Song, 2017; Song et al., 2012). To ensure reliable perception of visual objects in changing conditions, retinal adaptation exploits visual world similarities and differences (Song and Juusola, 2014; van Hateren, 1992b) through characteristic visual behaviors (Blaj and van Hateren, 2004; Juusola et al., 2017; Schilstra and Hateren, 1999) and employs costly codes (de Polavieja, 2002) through multiple layers of feedbacks. This gives emergence for *homeostatic* network gain regulation, in which photoreceptor adaptation is mediated both by intrinsic (Hardie and Juusola, 2015; Juusola and Hardie, 2001a; Song et al., 2012; Vähäsöyrinki et al., 2006) and synaptic feedbacks (Zheng et al., 2006; Zheng et al., 2009). Here, the absence of dSK, dSlo or both channels left the phototransduction cascade essentially intact but reduced the intrinsic photoreceptor *Shaker* and *Shab* conductances, which should have made voltage responses larger and slower. Yet, *in vivo* recordings refuted these predictions, showing instead distinctive mutation-specific dynamics. Therefore, the observed defects in photoreceptor adaptability - including response fluctuations and altered dynamic ranges - seem mostly attributable to the R-LMC-R system's suboptimally balanced synaptic feedforward inhibition and feedback excitation; reflecting homeostatic compensation at the network level. The resulting excitatory feedback overload also provided a plausible explanation why the mutant photoreceptors' resting potentials and response speeds differed from the wild-type (Abou Tayoun et al., 2011; Zheng et al., 2006).

The primary effects of mutations can be difficult to separate from the secondary effects of homeostatic compensation (Marder and Goaillard, 2006). Nonetheless, the overall consistency of our findings suggest that many differences in *in vivo* response properties of the mutants' R1-R6s and LMCs result from homeostatic gain regulation, whereupon differently balanced synaptic excitatory and inhibitory loads in the lamina network generate unique adaptive dynamics (encoding regimes); see also (Abbott and Lemasson, 1993; Lemasson et al., 1993). In the double-mutant, the most depolarized photoreceptors (Figure 2D) and the slowest LMC output (Figures 6D and 6E) imply that the network gain was particularly challenging to regulate, providing the most compromised adaptability and response range (Figure 7). In the single-mutants, adaptability of early vision was better compensated by enhanced network excitation, as seen by more wild-type-like LMC response dynamics (Figures 6C-E). But this still came with the cost of increased ATP consumption (Figures 5H and 5I). Moreover, in each case, the dSK and/or dSlo channel deletions affected optomotor behavior (Figure 7), suggesting that the mutants' distinct LMC output dynamics distorted their motion

perception; alike what we have previously shown to occur with different color channel mutants (Wardill et al., 2012). Here, *dSK*⁻ mutants' accelerated LMC responses (Figures 6B and 6C) presumably drove their fast hyper-saccadic optomotor responses (Figures 7A-D), while *dSlo*⁻ mutants' decelerated LMC responses (Figures 6B and 6C) most probably sensitized their vision to slow scene rotations (Figures 7A-D).

Summary

We have shown how Ca²⁺-activated K⁺ channels serve local and global neural communication, improving economics and adaptability. Locally, they help to reduce calcium load and repolarize membrane potentials in synaptic terminals. Globally, they reduce the overall network excitability and the cost of transmitting information, while increasing the range of neural adaptation and reliable perception.

In this study, we directly linked *in vivo* and *ex vivo* experiments with detailed stochastically operating biophysical models to extract new mechanistic knowledge of how *Drosophila* R-LMC-R circuitry homeostatically retains its information sampling and transmission capacity against perturbations in its ion-channel composition, and what is the cost of this compensation. We anticipate that this novel approach will provide a useful template to other model organisms and computational neuroscience, in general, in dissecting fundamental mechanisms of homeostatic compensation and deepening our understanding of how biological neural networks work.

STAR★METHODS

Key Resources Table

REAGENT or RESOURCE	SOURCE	IDENTIFIER
Experimental Models: Organisms/Strains		
<i>w</i> ⁺ ; +; <i>dSlo</i> ⁴	Gift from Nigel Atkinson laboratory	CG10693, FBgn0003429
<i>w</i> ⁺ ; +; <i>dSlo</i> ⁴ / <i>dSlo</i> ¹⁸	Gift from Allen Shearn laboratory	Dmel\ash2 ¹⁸ , FBal0057820
<i>w</i> ⁺ ; <i>dSK</i> ⁻ ; +	Patrick Dolph laboratory	CG10706, FBgn0029761
<i>w</i> ⁺ ; <i>dSK</i> ⁻ ; +; <i>dSlo</i> ⁴	In house	
<i>w</i> + <i>dSK</i> ⁻ ; +; <i>dSlo</i> ⁴ / <i>dSlo</i> ¹⁸	In house	
Maintained in the stock as:		
<i>w</i> ⁺ ; +; <i>Slo4</i> /TM6		
<i>w</i> + <i>dSK</i> ⁻ ; + ; +		
<i>w</i> + <i>dSK</i> ⁻ ; +; <i>dSlo</i> ⁴ /TM6		
<i>w</i> ⁺ ; +; <i>dSlo</i> ¹⁸ /TM6		

Software and Algorithms		
MATLAB-R2018B	MathWorks	https://www.mathworks.com/products/matlab.html
Biophysical <i>Drosophila</i> model (MATLAB)	github	https://github.com/JuusolaLab/Microsaccadic_Sampling_Paper/tree/master/BiophysicalPhotoreceptorModel
LMC feedback to R1-R6 estimation (MATLAB)	github	https://github.com/JuusolaLab/SK_Slo_Paper/tree/master/LMCFeedbackToR1-R6Model
Information estimation (MATLAB)	github	https://github.com/JuusolaLab/Microsaccadic_Sampling_Paper/tree/master/SNRAnalysis

Contact for Reagent and Resource Sharing

Further information and requests should be directed to and will be fulfilled by the Lead Contact Mikko Juusola (m.juusola@sheffield.ac.uk).

Experimental Model and Subject Details

***Drosophila melanogaster* rearing and strains.** The *dSK⁻* and *UAS-dSKDN* alleles were prepared as described earlier (Abou Tayoun et al., 2011). *Df7753* or *Df(1)Exel6290* line was obtained from Bloomington *Drosophila* stock center.

dSlo⁴ null allele (Atkinson et al., 1991) was kindly provided by Dr. Nigel Atkinson. *dSlo⁴* mutants appear often unhealthy, with the *dSlo* channel being expressed both in muscles and the brain (due to its 2 independent control regions), making them hesitant fliers (Atkinson et al., 2000). Therefore, we generated transheterozygotes *dSlo⁴/dSlo¹⁸*, facilitating the flight simulator experiments. *dSlo⁴* and *dSlo¹⁸* (also called *ash2¹⁸*) are both mutations of slowpoke (Atkinson et al., 2000; Lajeunesse and Shearn, 1995). But slowpoke has multiple promoters: *dSlo⁴* is a loss of function, whereas *dSlo¹⁸* affects promoter C0 and C1 (neural-specific) yet leaves C2 promoter intact. *dSlo¹⁸* produces a functional channel in the muscle, thereby mostly rescuing the flight deficits. *dSlo¹⁸* only affects the brain control region and is homozygous lethal, and thus, both *dSlo⁴* and *dSlo¹⁸* were maintained over a *TM6b* balancer. For experimental flies, *dSlo⁴/TM6* or *dSK⁻;dSlo⁴/TM6* were crossed to *dSlo¹⁸* and we selected against the *TM6* balancer. When combined in a *dSlo⁴/dSlo¹⁸*, the mutations only affects the expression of *dSlo* in the brain only. All the flies were previously outcrossed to a common Canton-S background, which was the wild-type control. The overall yield of *dSlo⁻* mutants was lower than for the other flies, with the surviving adults flies being typically smaller, which suggested that homozygotic *dSlo⁻* mutants were less healthy.

Drosophila were raised on molasses based food at 18 °C, under 12:12 h light:dark conditions. Prior to the experiments, the flies were moved to the laboratory (~21 °C) overnight or kept in a separate incubator at 25 °C. All electrophysiology (intracellular, electroretinogram and whole-cell recordings) was conducted at 20 ± 1 °C and optomotor behavior experiments at 21 ± 1 °C. During *in vivo* recordings, the fly temperature was feedback-controlled by a Peltier-system (Juusola et al., 2016; Juusola and Hardie, 2001b). Moreover, the theoretical model simulations of the R-LMC-R system (see below) were also calculated for 20 °C, by adjusting the Q₁₀ of phototransduction reactions and membrane properties accordingly (Juusola and Hardie, 2001b; Song et al., 2012). Thus, by retaining

effectively the same temperature for experiments and theory, we could compare directly the wild-type and mutant electrophysiology to their respective model predictions and optomotor behaviors.

Because the intracellular response dynamics of *dSlo*⁴ and *dSlo*⁴/*dSlo*¹⁸ R1-R6 photoreceptors and LMCs, respectively, appeared consistently similar, differing in the same way from the wild-type responses, these responses were pooled in the main results (Figures 1-7). For the same reason, the corresponding responses of *dSK*[;]*dSlo*⁴ and *dSK*[;]*dSlo*⁴/*dSlo*¹⁸ R1-R6 and LMCs were also pooled.

Electrophysiology and Analysis

Electroretinograms (ERGs). ERGs were recorded from intact flies following the standard procedures (Dau et al., 2016). ≤1 week old adult female *Drosophila* were fixed into a conical holder (Juusola et al., 2016; Juusola and Hardie, 2001a), using low melting point beeswax, and stimulated by 1 s light pulses from a green (560 nm) LED with the brightest effective intensity, estimated to be ~5 × 10⁶ effective photons/photoreceptor/s. Both recording and reference electrodes were filled with *Drosophila* ringer (in mM): 120 NaCl, 5 KCl, 1.5 CaCl₂, 4 MgCl₂, 20 proline, and 5 alanine. The recording electrode was positioned to touch the cornea and the indifferent electrode the head capsule near the ocelli. Recorded signals were low-pass filtered at 200 Hz and amplified via a npi SEC-10LX amplifier (npi Electronics, Germany).

A wild-type ERG comprises two main components: a slow component and transients coinciding with changes in light stimuli (Heisenberg, 1971). The slow component (or maintained background potential) is attributed to photoreceptor output and has the inverse waveform of photoreceptors' intracellular voltage responses, while on- and off-transients originate from the postsynaptic cells in the lamina (Coombe, 1986). We further plotted the ERGs as dynamic spectra (Figure 6H) to highlight how their oscillation frequencies changed in respect to light stimulation (Wolfram and Juusola, 2004).

Whole-Cell Recordings. Dissociated ommatidia were prepared from recently eclosed adult flies and transferred to a recording chamber on an inverted Nikon Diaphot microscope (Hardie et al., 2002). The control bath solution contained 120 mM NaCl, 5 mM KCl, 10 mM N-Tris-(hydroxymethyl)-methyl-2-amino-ethanesulphonic acid (TES), 4 mM MgCl₂, 1.5 mM CaCl₂, 25 mM proline, and 5 mM alanine. Osmolarity was adjusted to ~283 mOsm. The standard intracellular solution used in the recording pipette was composed of 140 mM K⁺ gluconate, 10 mM TES, 4 mM Mg²⁺ ATP, 2 mM MgCl₂, 1 mM NAD, and 0.4 mM Na⁺ GTP. Data were recorded with Axopatch 1-D or 200 amplifiers and analyzed with pClamp software (Axon Instruments). Cells were stimulated by a green-light-emitting diode with intensities calibrated in terms of effectively absorbed photons by counting quantum bumps at low intensities in wild-type flies.

In vivo intracellular recordings. 3-7 days old (adult) female flies were used in the experiments. A fly was fixed in a conical fly-holder with beeswax, and a small hole (6-10 ommatidia) for the recording microelectrode entrance was cut in its dorsal cornea and Vaseline-sealed to protect the eye (Juusola and Hardie, 2001a; Zheng et al., 2006). Sharp quartz and borosilicate microelectrodes (Sutter Instruments), having 120–200 MΩ resistance, were used for intracellular recordings from R1-R6 photoreceptors and large monopolar cells (LMCs). These recordings were performed separately; with the electrodes filled either with 3 M KCl solution for photoreceptor or 3 M potassium acetate with 0.5 mM KCl for LMC recordings, to maintain chloride battery. A reference electrode, filled with fly ringer, was gently pushed through ocelli ~100 μm into the head, in which temperature was kept at

19 ± 1°C by a feedback-controlled Peltier device (Juusola and Hardie, 2001b).

Only stable high-quality recordings were included. In darkness, R1-R6s' maximum responses to saturating bright pulses were characteristically >40 mV (wild-type, all mutants); the corresponding LMC recordings showed resting potentials <-30 mV and 10-40 mV maximum response amplitudes (wild-type and all mutants). Although the large maximum response variation is typical for *Drosophila* intracellular LMC recordings, their normalized waveforms characteristically display similar time-courses and dynamics (Nikolaev et al., 2009; Zheng et al., 2009). The smaller and more frequent responses are likely from LMC somata. These have larger diameters than the small and narrow LMC dendrites, in which responses should be the largest but the hardest to record from (Nikolaev et al., 2009; Wardill et al., 2012; Zheng et al., 2009). LMC subtypes were not identified, but most recordings were likely from L1 and L2 as these occupy the largest volume. Occasionally, we may have also recorded from other neurons or glia, which receive histaminergic inputs from photoreceptors (Rivera-Alba et al., 2011; Shaw, 1984; Zheng et al., 2006; Zheng et al., 2009). But because the selected recordings shared similar hyperpolarizing characteristics, LMC data for each genotype were analyzed together.

Light stimulation was delivered to the studied cells at center of its receptive field with a high-intensity green LED (Marl Optosource, with peak emission at 525 nm), through a fiber optic bundle, fixed on a rotatable Cardan arm, subtending 5° as seen by the fly. Its intensity was set by neutral density filters (Kodak Wratten) (Juusola and Hardie, 2001a); the results are shown for dim (estimated to be ~600), medium (~6 × 10⁴) and bright luminance (~6 × 10⁵ photons/s); or log -3, log -1 and log 0, respectively.

Voltage responses were amplified in current-clamp mode using 15 kHz switching rate (SEC-10L single-electrode amplifier; NPI Electronic, Germany). The stimuli and responses were low-pass filtered at 500 Hz (KemoVBF8), and sampled at 1 or 10 kHz. The data were re-sampled/processed off-line at 1-2 kHz for the analysis. Stimulus generation and data acquisition were performed by custom-written Matlab (MathWorks, Natick, MA) programs: BIOSYST (Juusola and de Polavieja, 2003; Juusola and Hardie, 2001a).

Data Analysis. The signal was the average of consecutive 1,000 ms long voltage responses to a repeated light intensity time series, selected from the naturalistic stimulus (NS) library (van Hateren, 1997), and its power spectrum was calculated using Matlab's Fast Fourier Transform (FFT) algorithm. First 10-20 responses were omitted because of their adaptive trends, and only approximately steady-state adapted responses were analyzed. The noise was the difference between individual responses and the signal, and its power spectra were calculated from the corresponding traces (Juusola et al., 1994). Thus, n trials (with n = 20), gave one signal trace and n noise traces. Both signal and noise data were chunked into 50% overlapping stretches and windowed with a Blackman-Harris-term window, each giving three 500-point-long samples. This gave 60 spectral samples for the noise and three spectral samples for the signal, which were averaged, respectively, to improve the estimates. $SNR(f)$, of the recording or simulation was calculated from their signal and noise power spectra, $\langle |S(f)|^2 \rangle$ and $\langle |N(f)|^2 \rangle$, respectively, as their ratio, where $||$ denotes the norm and $\langle \rangle$ the average over the different stretches (Juusola and de Polavieja, 2003; Juusola and Hardie, 2001a; Song and Juusola, 2014).

Information transfer rates, R , for each recording were estimated by using the Shannon formula (Shannon, 1948), which has been shown to obtain robust estimates for these types of continuous signals (Juusola et al., 2017; Juusola and de Polavieja, 2003; Song and Juusola, 2014). We analyzed steady-state-adapted recordings and simulations, in which each response (or stimulus trace) is expected to be equally representative of the underlying encoding (or statistical) process. From $SNR(f)$, the information transfer rate estimates were calculated as follows:

$$R = \int_2^{500 \text{ Hz}} \log_2(SNR(f) + 1) df \quad (1)$$

with the integral upper and lower bounds resulting from 1 kHz sampling rate and 500 points window size, respectively. The underlying assumptions of this method and how the number and resolution of spectral signal and noise estimates and the finite size of the used data can affect the resulting information transfer rate estimates have been analyzed before (Juusola and de Polavieja, 2003; Song and Juusola, 2014; van Hateren, 1992a) and are further discussed in (Juusola et al., 2017).

Using some longer recording series (to 50 stimulus repetitions), we further tested these R estimates against those obtained by the triple extrapolation method (Juusola and de Polavieja, 2003). This method, unlike SNR analysis, requires no assumptions about the signal and noise distributions or their additivity. Voltage responses were digitized by sectioning them into time intervals, T , that were subdivided into smaller intervals $t = 1$ ms. In the final step, the estimates for the entropy rate, R_S , and noise entropy rate, R_N , were then extrapolated from the values of the experimentally obtained entropies to their successive limits, as in (Juusola and de Polavieja, 2003):

$$R = R_S - R_N = \lim_{T \rightarrow \infty} \frac{1}{T} \lim_{v \rightarrow \infty} \lim_{size \rightarrow \infty} (H_S^{T,v,size} - H_N^{T,v,size}) \quad (2)$$

where T is the length of the ‘words’, v the number of voltage levels (in digitized amplitude resolution) and the *size* of the data file. The difference between the entropy and noise entropy rates is the rate of information transfer, R (Juusola and de Polavieja, 2003; Shannon, 1948). Again, as shown before for comparable data (Dau et al., 2016; Juusola et al., 2017; Song and Juusola, 2014), both methods gave similar R estimates, implying that the Shannon method (Eq. 1) estimates were unbiased.

As expected, information transfer rates at 20 °C were lower (Figure 4F) than those at 25 °C (Juusola et al., 2017; Song and Juusola, 2014), which is *Drosophila*’s preferred temperature (Sayeed and Benzer, 1996). Presumably, because of the tightly-compartmentalized enzymatic reactions inside each of its 30,000 microvilli (phototransduction/photon sampling units), the Q_{10} of a *Drosophila* R1-R6’s information transfer is high for many light stimuli; ≥ 4 for bright 200 Hz Gaussian white-noise stimulation (Juusola and Hardie, 2001b). Whereas, the Q_{10} of simple diffusion-limited reactions, such as ion channel currents, is lower, ~ 2 (Juusola and Hardie, 2001b; Lamb, 1984). Critically here, stochastic R1-R6 model simulations imply that warming accelerates microvilli recovery from their previous light-activation by shortening their refractory period (Song and Juusola, 2014). Therefore, for many bright fast-changing light patterns, a warm R1-R6 transduces characteristically more photons to quantum bumps than a cold one. And, with more bumps summing up bigger and faster macroscopic responses, extending their reliability to higher stimulus frequencies, information transfer increases (Juusola et al., 2016; Juusola and Hardie, 2001b; Juusola and Song, 2017).

Behavioral Experiments and Analysis

In the flight simulator experiments, we used 3-7 days old female flies, reared in 12:12 h dark:light

cycle. A flying fly, tethered from the classic torque-meter (Tang and Guo, 2001), which fixed its head in a rigid position and orientation, was lowered by a manipulator in the center of a black-white cylinder (spectral full-width: 380-900 nm). It saw a continuous (360°) stripe-scene. After viewing the still scene for 1 s, it was spun to the counter-clockwise by a linear stepping motor for 2 s, stopped for 2 s, before rotating to clock-wise for 2 s, and stopped again for 1 s. This 8 s stimulus was repeated 10 times and each trial, together with the fly's yaw torque responses, was sampled at 1 kHz and stored for later analysis (Wardill et al., 2012). Flies followed the scene rotations, generating yaw torque responses (optomotor responses to right and left), the strength of which presumably reflects the strength of their motion perception (Götz, 1964). The moving stripe scenes had: azimuth $\pm 360^\circ$; elevation $\pm 45^\circ$; wavelength 14.4° (coarse) and 3.9° (fine-grained = hyperacute); contrast 1.0, as seen by the fly. The scene was rotated at $45^\circ/\text{s}$ (slow) of $300^\circ/\text{s}$ (fast).

Biophysical Models for Estimating Wild-type and Mutant R1-R6s' Energy Consumption

Our published *Drosophila* photoreceptor model was used to simulate both the wild-type and mutant voltage responses to naturalistic light intensity time series (Song et al., 2012). It has four modules: (1) random photon absorption model, which regulates photon absorptions in each microvillus, following Poisson statistics; (2) stochastic quantum bump (QB) model, in which stochastic biochemical reactions inside a microvillus captures and transduces the energy of photons to variable QBs or failures (compare Figure 1B); (3) summation model, in which QBs from 30,000 microvilli integrate the macroscopic light-induced current (LIC) response; and (4) Hodgkin–Huxley (HH) model of the photoreceptor plasma-membrane, which transduces LIC into voltage response (see Figure 5B).

Modules 1-3 simulate the stochastic phototransduction cascade in the rhabdomere. Because the mutants' phototransduction reactions were physiologically intact (Figure 3), all the parameters were fixed and kept the same in the simulations; details in (Song et al., 2012). Module 4 models the R1-R6 plasma membrane using deterministic continuous functions (HH model), in which parameters scale the model response to light stimulation, approximating the recorded response.

Estimating ATP Consumption for Information Transmission in Wild-type and Mutant R1-R6s

While the microvilli, which form the photosensitive R1-R6 rhabdomere (Figure 1B), generate the LIC, the photo-insensitive plasma membrane uses many voltage-gated ion channels to adjust the LIC-driven voltage responses. In response to LIC, these open and close, regulating the ionic flow across the plasma membrane. But to maintain the pertinent ionic concentrations in- and outside, R1-R6s rely upon other proteins, such as ion cotransporters, exchangers and pumps, to uptake or expel ions. The work of moving ions against their electrochemical gradients consumes energy (ATP), and a R1-R6's ATP consumption thus much depends on the ionic flow dynamics through its ion channels (Laughlin et al., 1998). To approximate these dynamics during light responses, we used our HH R1-R6 body model (Niven et al., 2003; Song et al., 2012), which models the ion channels as conductances.

The HH model has these ion transporters: $3\text{Na}^+/2\text{K}^+$ -pump, $3\text{Na}^+/\text{Ca}^{2+}$ -exchanger and $\text{Na}^+/\text{K}^+/2\text{Cl}^-$ mechanisms to balance the intracellular ionic fluxes. $\text{Na}^+/\text{K}^+/2\text{Cl}^-$ cotransporter balances with the voltage-dependent Cl^- and Cl^- leak conductances, maintaining intracellular Cl^- concentration. Ca^{2+} influx in the LIC ($\sim 41\%$) is then expelled by $3\text{Na}^+/\text{Ca}^{2+}$ -exchanger in 1:3 ratio in exchange for Na^+ ions. Although there is K^+ influx in LIC ($\sim 24\%$), this is not enough to compensate K^+ leakage through

voltage-gated K^+ conductances and K^+ leaks. Apart from a small amount of K^+ intake through $Na^+/K^+/2Cl^-$ -cotransporter, $3Na^+/2K^+$ -pump is the major K^+ uptake mechanism. It consumes 1 ATP molecule to uptake 2 K^+ ions and extrudes 3 Na^+ ions. Because it is the major energy consumer in the cell, we use only the pump current (I_p) to estimate the ATP consumption. For these estimates, we generated two separate photoreceptor membrane models: a conservative one (Table S1; containing the known voltage-sensitive and leak potassium conductances; used in Figures 5 and S2) and a speculative one (Table S2; by adding an unconfirmed chloride conductance and leak, now balanced with larger voltage-sensitive K^+ conductances; Figure S3). Their differences helped us to work out how the earlier proposed hypothetical homeostatic compensation through leak- or chloride channel expression (Niven et al., 2003; Vähäsöyrinki et al., 2006) would change a photoreceptor's ATP consumption.

From the equilibrium of K^+ fluxes, I_p can be calculated as follows:

$$I_p = \frac{1}{2}(I_{Shaker} + I_{Shab} + I_{new} + I_{K_leak} - I_{LIC_K}) - \frac{1}{4}(I_{Cl} + I_{Cl_leak}) \quad (3)$$

where I_{Shaker} , I_{Shab} , I_{new} , and I_{K_leak} are the currents through Shaker, Shab, new, and K_leak channels, respectively, I_{LIC_K} is the K^+ influx in LIC and I_{Cl} and I_{Cl_leak} are the currents through the voltage-gated Cl^- and Cl^- leak channels, respectively. These currents can be calculated from the reverse potential of individual ions and their HH model produced conductances using Ohm's law:

$$I_{Shaker} = (E_m - E_K)g_{shaker} \quad (4)$$

$$I_{Shab} = (E_m - E_K)g_{shab}$$

$$I_{new} = (E_m - E_K)g_{new}$$

$$I_{K_leak} = (E_m - E_K)g_{K_leak}$$

$$I_{Cl} = (E_m - E_K)g_{Cl}$$

$$I_{Cl_leak} = (E_m - E_K)g_{Cl_leak}$$

Using I_p , the number of ATP molecules hydrolyzed per second can be calculated:

$$\frac{ATP_{molecules}}{s} = \frac{\int_0^T I_p dt}{T} \times \frac{N_A}{F} \quad (5)$$

where N_A is Avogadro's constant and F is Faraday's constant. The ATP usage per bit of information was calculated by dividing the estimated ATP molecules hydrolyzed in 1 s by the estimated information transfer rates (bits/s). We did not model the respective pump dynamics because, for the purpose of calculating ATP, only the time-integrated ionic fluxes count, not the time constants.

Previously, because of lack of a complete model for the photosensitive membrane, the LIC has only been estimated at the steady-state, or DC (Laughlin et al., 1998; Niven et al., 2007), when the sum of all currents across the model membrane equals zero:

$$I_{Shaker} + I_{Shab} + I_{new} + I_{K_leak} + I_{Cl} + I_{Cl_leak} + I_p + I_{LIC_K} = 0 \quad (6)$$

Thus here, the conservative photoreceptor membrane model (Table S1) lacked I_{Cl_leak} and I_{Cl} in Eqs. 3, 4 and 6, whereas the speculative model (Table S2) included them. But for both membrane models, because we estimated LIC directly from the stochastic phototransduction model (above), we could calculate a R1-R6's energy cost in response to any arbitrary light pattern, including naturalistic stimulation (Figure 5). Thus, our phototransduction cascade model provides the *functional* equivalence to the light-dependent conductance used in the previously published steady-state models (Laughlin et al., 1998; Niven et al., 2007).

Histology

Electron Microscopy. 3-to-7-day-old dark/light-reared *Drosophila* were cold anesthetized on ice and transferred to a drop of pre-fixative [modified Karnovsky's fixative: 2.5% glutaraldehyde, 2.5% paraformaldehyde in 0.1 M sodium cacodylate buffered to pH 7.3 – as per (Shaw et al., 1989)] on a transparent agar dissection dish. Dissection was performed using a shard of a razor blade (Feather S). Flies were restrained on their backs with insect pins through their lower abdomen and distal proboscis. Their heads were severed, proboscis excised, and halved. The left half-heads were collected in fresh pre-fixative and kept for 2 h at room temperature (21 ± 1 °C) under normal lighting conditions.

After pre-fixation, the half-heads were washed (2×15 min) in 0.1 M Cacodylate buffer, and then transferred to a 1 h post-fixative step, comprising Veronal Acetate buffer and 2% Osmium Tetroxide in the fridge (4°C). They were moved back to room temperature for a 9 min wash (1:1 Veronal Acetate and double-distilled H₂O mixture), and serially dehydrated in multi-well plates with subsequent 9 min washes in 50, 70, 80, 90, 95, and $2 \times 100\%$ ethanol.

Post-dehydration, the half-heads were transferred to small glass vials for infiltration. They were covered in Propylene Oxide (PPO) for 2×9 min, transferred into a 1:1 PPO:Epoxy resin mixture (Poly/Bed® 812) and left overnight. The following morning, the half-heads were placed in freshly made pure resin for 4 h, and placed in fresh resin for a further 72 h at 60 °C in the oven. Fixation protocol was provided by Professor Ian Meinertzhagen (Dalhousie University, Canada).

Embedded half-heads were first sectioned (at 0.5 µm thickness) using a glass knife, mounted in an ultramicrotome (Reichert-Jung Ultracut E, Germany). Samples were collected on glass slides, stained using Toluidine Blue and observed under a light microscope. This process was repeated and the cutting angle was continuously optimized until the correct orientation and sample depth was achieved; stopping when approximately 40 ommatidia were discernible. The block was then trimmed and shaped for ultra-thin sectioning. The trimming is necessary to reduce cutting pressure on the sample-block and resulting sections, thus helping to prevent “chattering” and compression artifacts.

Ultra-thin sections (85 nm thickness) were cut using a diamond cutting knife (DiATOME Ultra 45°, USA), mounted and controlled using the ultramicrotome. The knife edge was first cleaned using a polystyrol rod to ensure integrity of the sample-blocks. The cutting angles were aligned and the automatic approach- and return-speeds set on the microtome. Sectioning was automatic and samples were collected in the knife water boat.

Sections were transferred to Formvar-coated mesh-grids and stained for imaging: 25 min in Uranyl Acetate; a double-distilled H₂O wash; 5 min in Reynolds' Lead Citrate (Reynolds, 1963); and a final double-distilled H₂O wash.

Conventional microscopy. Heads of 8-day-old dark/light-reared female and male flies were bisected, fixed, and embedded as explained previously (Chinchore et al., 2009). 1 µm eye cross sections were cut using a Sorvall ultra microtome MT-1 (Sorvall, CT), stained with toluidine blue, and inspected using a Zeiss Axioplan2 microscope. Digital images were taken using Optronics DEI-750 camera (Optronics) and MetaVue (Universal Imaging) software.

Quantification and Statistical Analysis

In all cases, significance was calculated using 2 tailed paired Student's t test. Specific p values and sample sizes are indicated in the relevant figure legends.

SUPPLEMENTAL INFORMATION

Supplemental Information includes three figures, two tables, and can be found with this article online at <https://doi.org/xxxx>.

ACKNOWLEDGMENTS

We thank Nigel Atkinson, Allen Shearn, and the Bloomington Stock Centers for reagents. We thank the members of the Juusola lab for discussions and critical readings of the manuscript. This work was supported by the following grants to MJ: Biotechnology and Biological Sciences Research Council (BB/H013849/1, BB/F012071/1 and BB/D001900/1), Engineering and Physical Sciences Research Council (EP/P006094/1), Leverhulme Trust (RPG-2012-567), Jane and Aatos Erkko Foundation, High-End Foreign Expert Grant by Chinese Government (GDT20051100004) and Beijing Normal University (Open Research Fund), and grants to RCH: Biotechnology and Biological Sciences Research Council (BB/M007006/1 and BB/J0092531/1).

AUTHOR CONTRIBUTIONS

This research was initiated by M.J., P.D. and R.C.H. Genetics: A.A.T., P.D. and F.B. Electrophysiology: X.L., A.D., D.R., A.N., L.Z., M.B., B.C., R.C.H. and M.J. Electron microscopy: S.D. Histology: P.D. Optomotor behavior: D.J. Modeling and data analyses: Z.S., A.D. and M.J. M.J., P.D. and R.C.H. designed the experiments. M.J. wrote the manuscript with all authors contributing in editing. M.J., P.D. and R.C.H. procured funding.

DECLARATION OF INTERESTS

The authors declare no competing interests.

REFERENCES

- Abbott, L.F., and Lemasson, G. (1993). Analysis of neuron models with dynamically regulated conductances. *Neural Comput* 5, 823-842.
- Abou Tayoun, A.N., Li, X., Chu, B., Hardie, R.C., Juusola, M., and Dolph, P.J. (2011). The *Drosophila* SK channel (dSK) contributes to photoreceptor performance by mediating sensitivity control at the first visual network. *J Neurosci* 31, 13897-13910.
- Atkinson, N.S., Brenner, R., Chang, W.M., Wilbur, J., Larimer, J.L., and Yu, J. (2000). Molecular separation of two behavioral phenotypes by a mutation affecting the promoters of a Ca-activated K channel. *J Neurosci* 20, 2988-2993.
- Atkinson, N.S., Robertson, G.A., and Ganetzky, B. (1991). A component of calcium-activated potassium channels encoded by the *Drosophila* slo locus. *Science* 253, 551-555.
- Becker, M.N., Brenner, R., and Atkinson, N.S. (1995). Tissue-specific expression of a *Drosophila* calcium-activated potassium channel. *J Neurosci* 15, 6250-6259.
- Blaj, G., and van Hateren, J.H. (2004). Saccadic head and thorax movements in freely walking blowflies. *J Comp Physiol A* 190, 861-868.
- Blondeau, J., and Heisenberg, M. (1982). The 3-dimensional optomotor torque system of *Drosophila Melanogaster* - studies on wildtype and the mutant optomotor-blind H31. *J Comp Physiol* 145, 321-329.
- Chinchore, Y., Mitra, A., and Dolph, P.J. (2009). Accumulation of rhodopsin in late endosomes triggers photoreceptor cell degeneration. *PLoS Genet* 5, e1000377.

- 1 Clark, B.D., Kurth-Nelson, Z.L., and Newman, E.A. (2009). Adenosine-evoked hyperpolarization of retinal ganglion cells
2 is mediated by G-protein-coupled inwardly rectifying K⁺ and small conductance Ca²⁺-activated K⁺ channel activation. J
3 Neurosci 29, 11237-11245.
- 4 Coombe, P.E. (1986). The large monopolar cells L1 and L2 are responsible for ERG transients in *Drosophila*. J Comp
5 Physiol A 159, 655-665.
- 6 Cover, T.M., and Thomas, J.A. (2006). Elements of information theory, 2nd edn (Hoboken, N.J.: Wiley-Interscience).
- 7 Dau, A., Friederich, U., Dongre, S., Li, X.F., Bollepalli, M.K., Hardie, R.C., and Juusola, M. (2016). Evidence for dynamic
8 network regulation of *Drosophila* photoreceptor function from mutants lacking the neurotransmitter histamine. Front
9 Neural Circuit 10, 1-22.
- 10 de Polavieja, G.G. (2002). Errors drive the evolution of biological signalling to costly codes. Journal of theoretical biology
11 214, 657-664.
- 12 Faber, E.S., Delaney, A.J., and Sah, P. (2005). SK channels regulate excitatory synaptic transmission and plasticity in the
13 lateral amygdala. Nat Neurosci 8, 635-641.
- 14 Faber, E.S., and Sah, P. (2003). Calcium-activated potassium channels: multiple contributions to neuronal function.
15 Neuroscientist 9, 181-194.
- 16 Fettiplace, R., and Fuchs, P.A. (1999). Mechanisms of hair cell tuning. Ann Rev Physiol 61, 809-834.
- 17 Freifeld, L., Clark, D.A., Schnitzer, M.J., Horowitz, M.A., and Clandinin, T.R. (2013). GABAergic lateral interactions
18 tune the early stages of visual processing in *Drosophila*. Neuron 78, 1075-1089.
- 19 Gonzalez-Bellido, P.T., Wardill, T.J., and Juusola, M. (2011). Compound eyes and retinal information processing in
20 miniature dipteran species match their specific ecological demands. Proc Natl Acad Sci U S A 108, 4224-4229.
- 21 Götz, K.G. (1964). Optomotor studies of the visual system of several eye mutants of the fruit fly *Drosophila*. Kybernetik
22 2, 77-92.
- 23 Grimes, W.N., Li, W., Chavez, A.E., and Diamond, J.S. (2009). BK channels modulate pre- and postsynaptic signaling at
24 reciprocal synapses in retina. Nat Neurosci 12, 585-592.
- 25 Hardie, R.C. (1989). A histamine-activated chloride channel involved in neurotransmission at a photoreceptor synapse.
26 Nature 339, 704-706.
- 27 Hardie, R.C. (1991a). Voltage-sensitive potassium channels in *Drosophila* photoreceptors. J Neurosci 11, 3079-3095.
- 28 Hardie, R.C. (1991b). Whole-cell recordings of the light-induced current in dissociated *Drosophila* photoreceptors -
29 evidence for feedback by calcium permeating the light-sensitive channels. Proc R Soc B-Biol Sci 245, 203-210.
- 30 Hardie, R.C., and Juusola, M. (2015). Phototransduction in *Drosophila*. Curr Opin Neurobiol 34, 37-45.
- 31 Hardie, R.C., Martin, F., Cochrane, G.W., Juusola, M., Georgiev, P., and Raghu, P. (2002). Molecular basis of
32 amplification in *Drosophila* phototransduction: Roles for G protein, phospholipase C, and diacylglycerol kinase. Neuron
33 36, 689-701.
- 34 Hardie, R.C., Voss, D., Pongs, O., and Laughlin, S.B. (1991). Novel potassium channels encoded by the Shaker locus in
35 *Drosophila* photoreceptors. Neuron 6, 477-486.
- 36 Hardie, R.C., and Weckström, M. (1990). 3 classes of potassium channels in large monopolar cells of the blowfly
37 *Calliphora vicina*. J Comp Physiol A 167, 723-736.
- 38 Heisenberg, M. (1971). Separation of receptor and lamina potentials in electroretinogram of normal and mutant
39 *Drosophila*. J Exp Biol 55, 85-100.
- 40 Hu, W., Wang, T., Wang, X., and Han, J. (2015). Ih channels control feedback regulation from amacrine cells to
41 photoreceptors. PLoS Biol 13, e1002115.
- 42 Joesch, M., Schnell, B., Raghu, S.V., Reiff, D.F., and Borst, A. (2010). ON and OFF pathways in *Drosophila* motion
43 vision. Nature 468, 300-304.
- 44 Juusola, M., Dau, A., Song, Z.Y., Solanki, N., Rien, D., Jaciuch, D., Dongre, S., Blanchard, F., de Polavieja, G.G., Hardie,
45 R.C., and Takalo, J. (2017). Microsaccadic sampling of moving image information provides *Drosophila* hyperacute vision.
46 Elife 6, e26117.

- 1 Juusola, M., Dau, A., Zheng, L., and Rien, D.N. (2016). Electrophysiological method for recording intracellular voltage
- 2 responses of *Drosophila* photoreceptors and interneurons to light stimuli *in vivo*. *Jove-J Vis Exp* 112, e54142.
- 3 Juusola, M., and de Polavieja, G.G. (2003). The rate of information transfer of naturalistic stimulation by graded potentials.
- 4 *J Gen Physiol* 122, 191-206.
- 5 Juusola, M., and Hardie, R.C. (2001a). Light adaptation in *Drosophila* photoreceptors: I. Response dynamics and
- 6 signaling efficiency at 25 degrees C. *J Gen Physiol* 117, 3-25.
- 7 Juusola, M., and Hardie, R.C. (2001b). Light adaptation in *Drosophila* photoreceptors: II. Rising temperature increases
- 8 the bandwidth of reliable signaling. *J Gen Physiol* 117, 27-42.
- 9 Juusola, M., Kouvalainen, E., Järvilehto, M., and Weckström, M. (1994). Contrast gain, signal-to-noise ratio, and linearity
- 10 in light-adapted blowfly photoreceptors. *J Gen Physiol* 104, 593-621.
- 11 Juusola, M., and Song, Z. (2017). How a fly photoreceptor samples light information in time. *J Physiol-London* 595,
- 12 5427-5437.
- 13 Juusola, M., Uusitalo, R.O., and Weckstrom, M. (1995). Transfer of graded potentials at the photoreceptor interneuron
- 14 synapse. *J Gen Physiol* 105, 117-148.
- 15 Juusola, M., and Weckström, M. (1993). Band-pass filtering by voltage-dependent membrane in an insect photoreceptor.
- 16 *Neurosci Lett* 154, 84-88.
- 17 Klocker, N., Oliver, D., Ruppersberg, J.P., Knaus, H.G., and Fakler, B. (2001). Developmental expression of the small-
- 18 conductance Ca(2+)-activated potassium channel SK2 in the rat retina. *Mol Cell Neurosci* 17, 514-520.
- 19 Kolodziejczyk, A., Sun, X., Meinertzhagen, I.A., and Nassel, D.R. (2008). Glutamate, GABA and acetylcholine signaling
- 20 components in the lamina of the *Drosophila* visual system. *PLoS One* 3, e2110.
- 21 Lajeunesse, D., and Shearn, A. (1995). Transregulation of thoracic homeotic selector genes of the antennapedia and
- 22 bithorax complexes by the trithorax group genes - absent, small, and homeotic Disc-1 and Disc-2. *Mech Develop* 53, 123-
- 23 139.
- 24 Lamb, T.D. (1984). Effects of temperature-changes on toad rod photocurrents. *J Physiol-London* 346, 557-578.
- 25 Laughlin, S.B., de Ruyter van Steveninck, R.R., and Anderson, J.C. (1998). The metabolic cost of neural information.
- 26 *Nat Neurosci* 1, 36-41.
- 27 Lemasson, G., Marder, E., and Abbott, L.F. (1993). Activity-dependent regulation of conductances in model neurons.
- 28 *Science* 259, 1915-1917.
- 29 Marder, E., and Goaillard, J.M. (2006). Variability, compensation and homeostasis in neuron and network function. *Nat*
- 30 *Rev Neurosci* 7, 563-574.
- 31 Meinertzhagen, I.A., and O'Neil, S.D. (1991). Synaptic organization of columnar elements in the lamina of the wild type
- 32 in *Drosophila melanogaster*. *J Comp Neurol* 305, 232-263.
- 33 Ngo-Anh, T.J., Bloodgood, B.L., Lin, M., Sabatini, B.L., Maylie, J., and Adelman, J.P. (2005). SK channels and NMDA
- 34 receptors form a Ca²⁺-mediated feedback loop in dendritic spines. *Nat Neurosci* 8, 642-649.
- 35 Nikolaev, A., Zheng, L., Wardill, T.J., O'Kane, C.J., de Polavieja, G.G., and Juusola, M. (2009). Network adaptation
- 36 improves temporal representation of naturalistic stimuli in *Drosophila* eye: II mechanisms. *PLoS One* 4, e4306.
- 37 Niven, J.E., Vähäsöyrinki, M., Kauranen, M., Hardie, R.C., Juusola, M., and Weckström, M. (2003). The contribution of
- 38 Shaker K⁺ channels to the information capacity of *Drosophila* photoreceptors. *Nature* 421, 630-634.
- 39 Pelucchi, B., Grimaldi, A., and Moriondo, A. (2008). Vertebrate rod photoreceptors express both BK and IK calcium-
- 40 activated potassium channels, but only BK channels are involved in receptor potential regulation. *J Neurosci Res* 86, 194-
- 41 201.
- 42 Raghu, S.V., and Borst, A. (2011). Candidate glutamatergic neurons in the visual system of *Drosophila*. *PLoS One* 6,
- 43 e19472.
- 44 Ramanathan, K., Michael, T.H., Jiang, G.J., Hiel, H., and Fuchs, P.A. (1999). A molecular mechanism for electrical tuning
- 45 of cochlear hair cells. *Science* 283, 215-217.
- 46 Rivera-Alba, M., Vitaladevuni, S.N., Mishchenko, Y., Lu, Z., Takemura, S.Y., Scheffer, L., Meinertzhagen, I.A.,

- 1 Chklovskii, D.B., and de Polavieja, G.G. (2011). Wiring economy and volume exclusion determine neuronal placement
- 2 in the *Drosophila* brain. *Curr Biol* 21, 2000-2005.
- 3 Sah, P. (1996). Ca(2+)-activated K⁺ currents in neurones: types, physiological roles and modulation. *Trends Neurosci* 19,
- 4 150-154.
- 5 Salkoff, L. (2006). A tail of multiple calcium-sensing domains. *J Gen Physiol* 128, 387-388.
- 6 Sayeed, O., and Benzer, S. (1996). Behavioral genetics of thermosensation and hygrosensation in *Drosophila*. *P Natl Acad*
- 7 *Sci USA* 93, 6079-6084.
- 8 Schilstra, C., and Hateren, J.H. (1999). Blowfly flight and optic flow. I. Thorax kinematics and flight dynamics. *J Exp*
- 9 *Biol* 202 (Pt 11), 1481-1490.
- 10 Shannon, C.E. (1948). A mathematical theory of communication. *Bell Syst Tech J* 27, 379-423.
- 11 Shatz, C.J. (1990). Competitive interactions between retinal ganglion cells during prenatal development. *J Neurobiol* 21,
- 12 197-211.
- 13 Shaw, S.R. (1984). Early visual processing in insects. *J Exp Biol* 112, 225-&.
- 14 Shaw, S.R., Frohlich, A., and Meinertzhagen, I.A. (1989). Direct connections between the R7/8 and R1-6 photoreceptor
- 15 subsystems in the *dipteran* visual-system. *Cell Tissue Res* 257, 295-302.
- 16 Song, Z., and Juusola, M. (2014). Refractory sampling links efficiency and costs of sensory encoding to stimulus statistics.
- 17 *J Neurosci* 34, 7216-7237.
- 18 Song, Z., and Juusola, M. (2017). A biomimetic fly photoreceptor model elucidates how stochastic adaptive quantal
- 19 sampling provides a large dynamic range. *J Physiol*.
- 20 Song, Z., Postma, M., Billings, S.A., Coca, D., Hardie, R.C., and Juusola, M. (2012). Stochastic, adaptive sampling of
- 21 information by microvilli in fly photoreceptors. *Curr Biol* 22, 1371-1380.
- 22 Stocker, M. (2004). Ca(2+)-activated K⁺ channels: molecular determinants and function of the SK family. *Nat Rev*
- 23 *Neurosci* 5, 758-770.
- 24 Tang, S., and Guo, A. (2001). Choice behavior of *Drosophila* facing contradictory visual cues. *Science* 294, 1543-1547.
- 25 Uusitalo, R.O., Juusola, M., and Weckström, M. (1995). Graded responses and spiking properties of identified first-order
- 26 visual interneurons of the fly compound eye. *J Neurophysiol* 73, 1782-1792.
- 27 Vähäsöyrinki, M., Niven, J.E., Hardie, R.C., Weckström, M., and Juusola, M. (2006). Robustness of neural coding in
- 28 *Drosophila* photoreceptors in the absence of slow delayed rectifier K⁺ channels. *J Neurosci* 26, 2652-2660.
- 29 van Hateren, J.H. (1992a). Theoretical predictions of spatiotemporal receptive-fields of fly LMCs, and experimental
- 30 validation. *J Comp Physiol A* 171, 157-170.
- 31 van Hateren, J.H. (1992b). A theory of maximizing sensory information. *Biol Cybern* 68, 23-29.
- 32 van Hateren, J.H. (1997). Processing of natural time series of intensities by the visual system of the blowfly. *Vision Res*
- 33 37, 3407-3416.
- 34 Wang, G.Y., Olshausen, B.A., and Chalupa, L.M. (1999). Differential effects of apamin- and charybdotoxin-sensitive K⁺
- 35 conductances on spontaneous discharge patterns of developing retinal ganglion cells. *J Neurosci* 19, 2609-2618.
- 36 Wardill, T.J., List, O., Li, X., Dongre, S., McCulloch, M., Ting, C.Y., O'Kane, C.J., Tang, S., Lee, C.H., Hardie, R.C., and
- 37 Juusola, M. (2012). Multiple spectral inputs improve motion discrimination in the *Drosophila* visual system. *Science* 336,
- 38 925-931.
- 39 Wolfram, V., and Juusola, M. (2004). Impact of rearing conditions and short-term light exposure on signaling performance
- 40 in *Drosophila* photoreceptors. *J Neurophysiol* 92, 1918-1927.
- 41 Xu, J.W., and Slaughter, M.M. (2005). Large-conductance calcium-activated potassium channels facilitate transmitter
- 42 release in salamander rod synapse. *J Neurosci* 25, 7660-7668.
- 43 Zettler, F., and Järvilehto, M. (1973). Active and passive axonal propagation of non-spike signals in retina of *Calliphora*.
- 44 *J Comp Physiol* 85, 89-104.
- 45 Zheng, L., de Polavieja, G.G., Wolfram, V., Asyali, M.H., Hardie, R.C., and Juusola, M. (2006). Feedback network
- 46 controls photoreceptor output at the layer of first visual synapses in *Drosophila*. *J Gen Physiol* 127, 495-510.

- 1 Zheng, L., Nikolaev, A., Wardill, T.J., O'Kane, C.J., de Polavieja, G.G., and Juusola, M. (2009). Network adaptation
- 2 improves temporal representation of naturalistic stimuli in *Drosophila* eye: I dynamics. PLoS One 4, e4307.
- 3